2012

Introduction of critical stress state criterion to predict bond strength between FRP and concrete substrate

Shigeyuki Ueno

INTRODUCTION OF CRITICAL STRESS STATE CRITERION TO PREDICT BOND STRENGTH BETWEEN FRP AND CONCRETE SUBSTRATE

by

SHIGEYUKI UENO

A DISSERTATION

Submitted in partial fulfillment of the requirements
for the degree of Doctor of Philosophy
in
The Department of Civil and Environmental Engineering
to
The School of Graduate Studies
of
The University of Alabama in Huntsville

HUNTSVILLE, ALABAMA

2012

In presenting this dissertation in partial fulfillment of the requirements for a doctoral degree from The University of Alabama in Huntsville, I agree that the Library of this University shall make it freely available for inspection. I further agree that the permission for extensive copying for scholarly purposes may be granted by my advisor or, in his/her absence, by the Chair of the Department or the Dean of the School of Graduate Studies. It is also understood that due recognition shall be given to me and to The University of Alabama in Huntsville in any scholarly use which may be made of any material in this dissertation.

Shigeyuki Mero
(student signature)

10/26/12
(date)

DISSERTATION APPROVAL FORM

Submitted by Shigeyuki Ueno in partial fulfillment of the requirements for the degree of Doctor of Philosophy in Civil Engineering and accepted on behalf of the Faculty of the School of Graduate Studies by the dissertation committee.

We, the undersigned members of the Graduate Faculty of The University of Alabama in Huntsville, certify that we have advised and/or supervised the candidate on the work described in this dissertation. We further certify that we have reviewed the dissertation manuscript and approved it in particular fulfillment of the requirements for the degree of Doctor of Philosophy in Civil Engineering.

G H A. Ronta Jr	11/1/2012 (Date)	Committee Chair
Ashraf Ghamdan	11/1/12	
Wilde Zero	11/1/12	
[signature]	11/1/12	
Jamal H Jawad for Dr. Uddin	11/1/12	
G H A. Ronta Jr		Department Chair
[signature]		College Dean
Rhonda Kay Gaede	11/14/12	Graduate Dean

ABSTRACT
The School of Graduate Studies
The University of Alabama in Huntsville

Degree Doctor of Philosophy College/Department Engineering / Civil and Environmental Engineering

Name of Candidate Shigeyuki Ueno

Title Introduction of Critical Stress State Criterion to Predict Bond Strength between FRP and Concrete Substrate

The technique of externally bonded FRP to existing concrete structures has been rapidly growing in the civil engineering field. In general, the performance of the strengthened structures depends on the bond between FRP and concrete. The development of conceptual predicting expression for the bond strength capturing the debonding initiation and behavior is needed. Prediction models are developed as a function of material properties of structures with empirical and mathematical coefficients and parameters. Analyzing and understanding the debonding mechanism enables the FRP strengthening technique more wide-use and application. Study of debonding behavior is the main focus of this research.

A simple criterion for the FRP debonding initiation is proposed. Using the elasticity theory, the critical stress state on a finite element in the vicinity of the bond interface is considered to develop an analytical solution. The shear-slip behavior at the bond interface is described with the developed analytical solution based on mechanics of materials. The adhesive material properties are successfully implemented as well as the properties of FRP and concrete substrate. The fracture depth and the strength factor are established from a single pull-off test. The proposed criterion and the analytical solution

are then applied to the experiment conducted in this study and existing experimental data from literature (totally 342 data points), to predict the bond strength. The comparison between predicted values and experimental data shows good agreement providing a relatively high correlation factor. In addition, comparison between the existing models and the proposed model verifies the validity of the proposed criterion and the predicting expressions.

Abstract Approval: Committee Chair 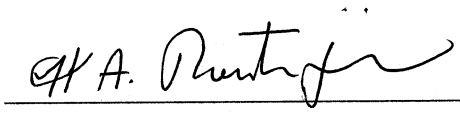

Department Chair 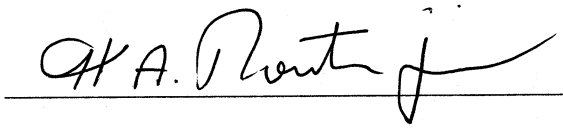

Graduate Dean 

ACKNOWLEDGEMENT

I would like to express my appreciation to my advisor, Dr. Houssam Toutanji, for his continuous support, encouragement, and patience that enabled me to pursue the degree. I would also like to express my gratitude to the department faculty and my committee members for providing support and guidance. This research would not have been possible without their invaluable support for years. Special thanks for support from all my graduate student friends, especially Mr. Dong Wang, Mr. Hyungjoo Choi, and Mr. Rajesh Vuddandam, for helping with the experimental work and sharing literature and thoughts with me.

I would like to convey my sincere gratitude to my family for their continuous understanding and support throughout the duration of my studies.

TABLE OF CONTENTS

LIST OF FIGURES

LIST OF TABLES

LIST OF SYMBOLS

A	a coefficient related to adhesive stiffness
b_c	width of concrete substrate
b_p	width of FRP strip
b_0	a function in terms of reference thickness
B	a coefficient related to stiffness of FRP and adhesive thickness
C	a function of applied load level with exponential terms
C_1	a coefficient for a solution
C_2	a coefficient for a solution
C_f	a constant related to fracture energy and concrete tensile strength
d	distance from loaded end to considered element
dx	differential distance in FRP interface
$d\sigma_1$	differential compressive stress on element in adhesive
$d\sigma_2$	differential tensile stress on element in adhesive
D	a function of position with exponential terms
E	a function of position with exponential terms
E_a	Young's modulus of epoxy
E_p	Young's modulus of FRP
f_b	limit bond stress for FRP debonding
f_c'	concrete compressive strength
f_{cu}	cube concrete compressive strength
f_t	concrete tensile strength

G_a	shear modulus of adhesive
G_f	interfacial fracture energy
H	horizontal surface load
k	an empirical constant
k_b	a factor related to width ratio of FRP to concrete substrate
k_c	a parameter presenting level of concrete surface preparation
K	a coefficient relating to properties of FRP and adhesive
l	shear deformation of adhesive layer due to interfacial shear stress
L	bond length
L_e	effective bond length
n	a descending controlling parameter
P_{app}	actual level of applied load
$P_{\text{app\_}\tau\text{max}}$	applied load corresponding to maximum interfacial shear stress
P_{max}	maximum transferable load
r	radial distance from a point to object
s	FRP local slip
s_u	ultimate slip
s_0	slip corresponding to maximum interfacial shear stress
t	fracture depth
t_a	thickness of epoxy layer
t_p	thickness of FRP strip
t_{ref}	reference thickness of concrete substrate
x	point on bond length

α	a strength factor relating to concrete compressive strength
α_{avg}	an average strength factor of α_1 and α_2
α_1	a strength factor for 1st set of concrete substrate
α_2	a strength factor for 2nd set of concrete substrate
β_p	a function of width ratio of FRP to concrete substrate
β_l	a coefficient related to effective bond length
β_L	a coefficient related to effective bond length
β_w	a factor related to width ratio of FRP to concrete substrate
γ_a	shear deformation angle of adhesive layer
δ	axial elongation of adhesive at interface to FRP
θ	radial angle measured from vertical line to radial positioning line
θ_1	transformation angle
θ_2	angle measured from vertical line at a point to radial positioning line
θ_3	angle measured from vertical line at loaded end to radial positioning line
σ_a	axial stress in adhesive at interface to FRP
σ_e	stress state in an element
$\sigma_{e,d}$	stress state in an substrate element at certain depth and distance
σ_p	axial stress in FRP strip
τ	interfacial shear stress
τ_{max}	maximum interfacial shear stress
λ	roots for characteristic equation of 2nd order differential equation
λ_1	a positive root of characteristic equation of ODE on bond behavior
λ_2	a negative root of characteristic equation of ODE on bond behavior

v_a	Poisson's ratio of adhesive
Δb_p	width related to the effect of bonded area

CHAPTER I

INTRODUCTION

1.1 FRP Background

For existing deficient concrete infrastructures such as beams, decks, slabs, walls, and columns strengthening methods have been the common practice by using various conventional materials instead of replacing them by completely new structures. One of the increasingly used materials for strengthening purpose is fiber reinforced polymers (FRP) composites consisting of fiber (carbon, aramid, or glass) and adhesive epoxy resin matrix. FRP sheets or plates are externally bonded to surfaces, especially tension faces, of concrete structures with adhesive materials. Fibers are anisotropic and fabricated into various forms, such as unidirectional, plain weave, chopped mat, and woven rovings to achieve appropriate mechanical properties as strengthening materials. Epoxy resin is the most common polymer matrix with high mechanical strength and good bonding to materials such as metal and glass. As a retrofitting component, FRP has many advantages over other conventional materials such as steel. It is light weight, corrosion resistant, non-magnetic, and has a relatively high strength in tension. In addition, FRP installation saves time and labor with the easy execution processes without using heavy equipment [1].

Historical records show that the first application of externally bonded steel plate as reinforcement to buildings and bridges was 50 years ago. The development of FRP application technique to infrastructures such as reinforced concrete started in Europe in the 1980's [2]. As structural engineers began to study design criteria and various FRP applications, more research on FRP reinforcement was conducted in the 1990's. During that period, the international symposium contributed the development of retrofitting concrete structures with FRP [3].

In general, the effectiveness of FRP reinforced concrete structures depends on the bond strength between FRP and concrete substrate. The bond interface is commonly considered as the critical part of the FRP bond system where debonding initiates before the ultimate strength of FRP is reached. Therefore, understanding the bond behavior and the mechanics of stress transfer with the corresponding deformation under a certain loading level is essential for engineers to predict the structural performance. Many experimental studies have been carried out to study such bond behavior and to develop bond strength prediction models. A single pull-off test (or a single shear test) is widely used to characterize the bond strength and the maximum transferable load of the FRP composites and the substrate. The bond strength prediction models available in literature can be classified into three types: empirical models, theoretical models, and the combination of the two models. Empirical prediction models have the maximum transferable load expressions based on experimental results and usually in simple forms. In contrast, theoretical models are derived based on the fracture mechanics theory on the bond interface, and some models include analytical solutions describing the bond behavior by using mechanics of materials. In those expressions, some coefficients are

added and determined with regression analysis or finite element analysis. Models combining those empirical and theoretical approaches are mostly studied by many authors to have fracture mechanics-based forms with empirical parameters bridging between theory and practice.

1.2 Problem Statement

For the global application of bond strength prediction models, a theoretical and conceptual approach for FRP debonding is needed without limitation of specific structural setups and type of adhesive materials. In most prediction models, the bond strength is expressed as a function of concrete and FRP material properties. The effect of adhesive material is often ignored even though its considerable thickness and stiffness could influence the bond strength of composite materials. The effect of adhesive properties is considered in a few expressions predicting the FRP debonding. A large number of experimental data with variety of material types and test setups are required to quantify the effect of adhesive parameters in bond strength expression. In theoretical models, these parameters tend to be implemented in complicated forms.

The bond strength expressions from most prediction models are in expanded forms of a fundamental expression in terms of interfacial fracture energy based on non-linear fracture mechanics. The interfacial fracture energy of FRP debonding tend to be determined with empirical expressions, and in this study, its expression is theoretically derived by considering the mechanism of FRP debonding initiation and the bond interfacial behavior corresponding to the subjected load level. With such theoretical expression, the performance of structures with externally bonded FRP reinforcement is predictably independent on material types or structural configurations.

1.3 Objectives

Applying a theoretical approach to describe the bond behavior under a certain load level and to predict the bond strength between FRP and concrete substrate is the main objective of this research. The detailed objectives are as follows:

(1) Propose a simple stress state criterion for FRP debonding initiation based on concrete tensile strength.

(2) Determine strength coefficients to modify concrete tensile strength using regression analysis.

(3) Determine the expression for the stress state on a finite element in concrete substrate at a certain position as a function of the interfacial shear stress distribution by using the elasticity theory.

(4) Determine a fracture depth in which FRP debonding initiates through experimental measurements.

(5) Obtain expressions for the interfacial shear distribution and local slip at a certain loading level by developing an analytical solution comprising adhesive material properties as parameters.

(6) Obtain the numerical values for the maximum interfacial shear stress and the corresponding local slip by applying the proposed criterion.

(7) Perform a single pull-off test for FRP to concrete composite to predict the maximum transferable load.

(8) Verify the proposed criterion using existing experimental data sets.

(9) Investigate the performance of the proposed theoretical criterion with existing prediction models.

1.4 Outlines of the Dissertation

Chapter II provides a brief review on the use of FRP composites in civil engineering structures, background of FRP debonding analysis, and existing models from literature. Chapter III contains a mathematical framework for the derivation of an analytical solution to predict the bond strength and behavior using a proposed critical stress criterion. Chapter IV shows numerical analysis of the proposed expression using an existing single pull-off test data set. Chapter V presents the experimental program of a single pull-off test. Chapter VI analyzes the experimental results to determine the fracture depth and the strength factor, and compares prediction values from the proposed expression and existing prediction models with existing and the conducted experimental data sets. Chapter VII summarizes and concludes the work.

CHAPTER II

LITERATURE REVIEW

2.1 FRP Implementation History

In the US, the FRP type reinforced resin matrix material was first used in the early 1940's [4]. Before and after World War II, most of the applications of fiberglass were for the military and aerospace fields as they are corrosive resistance and light weight. The first commercially manufactured composite product was a boat hull in marine fields. In the 1970's, the composite material demand in automobile industries surpassed marine markets. Besides glass fibers, the commercialization of aramid and carbon FRP grew enormously [5]. Although after the Cold War the demand for carbon fiber in the military decreased, the recreation industry expanded the carbon FRP usage into sporting goods. Industries such as the aerospace, energy efficiency, construction, and others explored FRP implementation.

In the civil engineering field, the first application of modern composite materials was found in a dome structure at Benghazi in 1968. During the 1970's to 1980's, many applications of FRP as reinforcing infrastructures were performed in Europe and Asia. In 1982, a FRP bridge deck was installed in China. In 1986, FRP as reinforcing bar was

used to construct a bridge in Germany. In the US, a FRP reinforced bridge deck was first built in McKinleyville, West Virginia, followed by an all FRP vehicular bridge deck in Russell, Kansas. For rehabilitation purposes, externally bonded steel plate was introduced to existing infrastructures and studied first in the 1960's [6]. Further research on practical applications of the reinforcement method was conducted in many countries and institutes ([7]-[11]). In the mid-1980's, FRP sheets were introduced to replace steel plates [12]. Since then, a number of studies were done on externally bonded FRP ([13]-[21]).

The composite institutes reported that the transportation industry had 31% of the market share, and FRP were mainly used for the maintenance and rehabilitation of existing concrete infrastructures [22]. Evaluating the capacity of reinforced structures has been the main research topic for better design safety on practical applications.

2.2 Basics of FRP Debonding Analysis

FRP composite materials have several advantages over conventional materials. They are used for rehabilitation and retrofitting applications due to their light weight and high strength. In civil engineering applications, carbon fiber is commonly applied as the external reinforcement to strengthen flexural members due to its high resistance against tensile stress. Epoxy resins are used as adhesive to embed fibers in the matrix system and to bond FRP to concrete substrate. Table 2.1 shows the comparison of the specific gravity, ultimate tensile strength, and Young's modulus of conventional metallic materials, three types of fibers, and FRP composite materials.

Table 2.1 Properties of Typical Fibers and Metals

Material	Specific gravity	Ultimate strength (MPa)	Young's modulus (GPa)
Steel	7.8	648	207
Aluminum	2.6	276	69
Graphite fiber	1.8	2067	230
Aramid fiber	1.4	1379	124
Glass fiber	2.5	1550	85
Unidirectional graphite/epoxy	1.6	1500	181
Unidirectional glass/epoxy	1.8	1062	39

Many studies on external FRP reinforcement to tension surfaces were carried out to analyze failure types ([23]-[26]). Several failure modes were classified based on crack propagation and crack type in concrete substrate ([25]-[27]). Figure 2.1 shows some of the failure modes: (a) cover separation, (b) plate end interfacial debonding, (c) intermediate flexure crack-induced interfacial debonding, and (d) intermediate flexure-shear crack-induced interfacial debonding. Figure 2.1 (a) and (b) are more common failures and in order to simulate and assess the stress state of such failures, various forms of pull-off tests are widely used. A single pull-off test is a simple method conducted by many authors and Figure 2.2 illustrates the test configuration. Material properties shown in the figure are the transferable load P_{app}, Young's modulus E_p and E_a, thickness t_p and t_a, width b_p, and the bond length L where subscripts p and a correspond to FRP and adhesive, respectively. One end of the adhesive layer close to the applied load is denoted as the loaded end and the other as the free end.

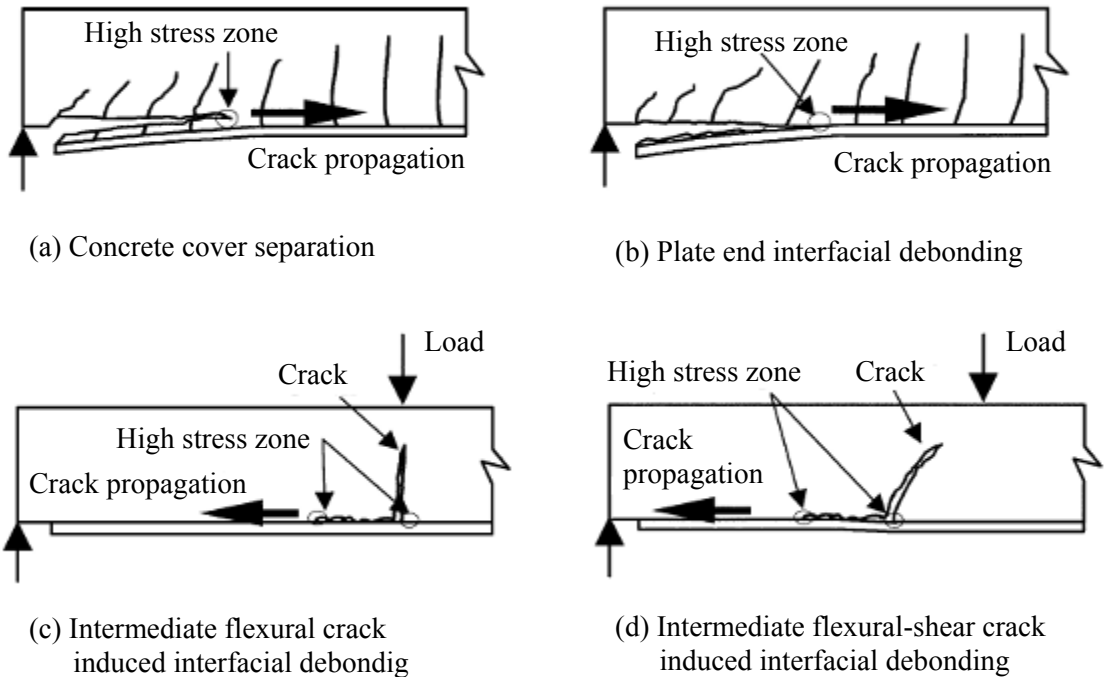

Figure 2.1 Failure Modes of RC Beams Reinforced Externally Bonded FRP [25]

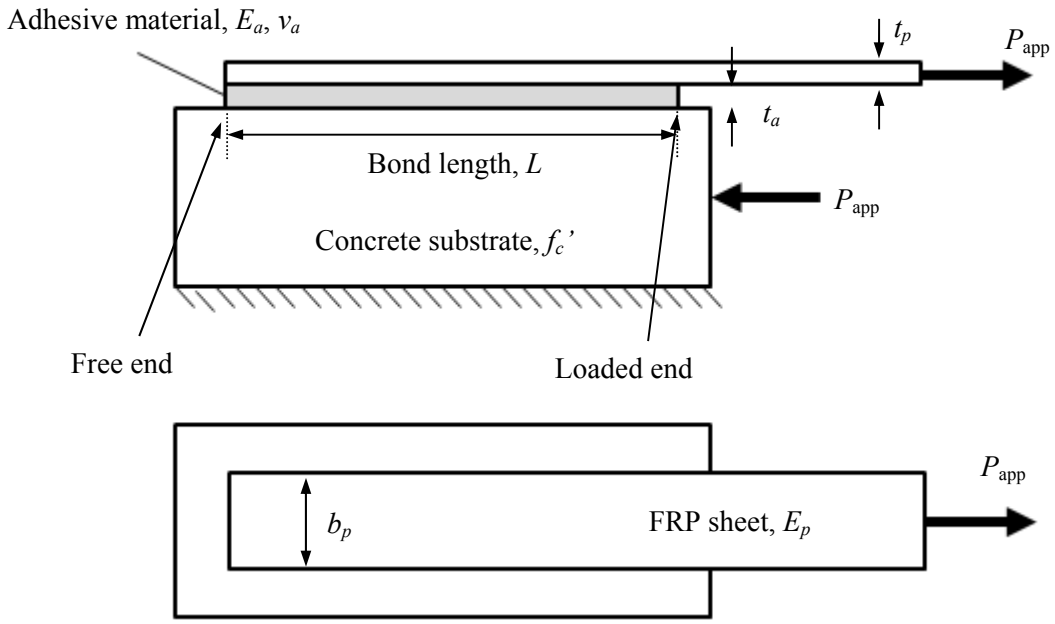

Figure 2.2 Sketch of Single Pull-off Test for FRP to Concrete

The transferable load P_{app} is the load applied to one end of the FRP sheet bonded to concrete substrate as shown in Figure 2.2, and the maximum transferable load, which is commonly denoted as P_{max}, is obtained through the test as the bond strength of the composite structure. In the analysis, the shear stress in the bond interface and the FRP relative slip to concrete substrate are determined to describe the bond behavior under tensile stress ([28]-[35]). These shear stress and slip are commonly denoted as the interfacial shear stress, τ, and the local slip, s (Figure 2.3). Usually, these parameters are related to yield a shear-slip curve. Based on experimental and analytical measurements, several types of shear-slip curves are proposed: (a) linear, (b) bi-linear, and (c) non-linear as shown in Figure 2.4. Three parameters, the maximum interfacial shear stress τ_{max}, the

slip s_0 at the maximum shear stress, and the ultimate slip s_u, characterize the bond behavior and the curve shape. Linear and bi-linear models are simple and easy to apply for bond behavior analysis. Several studies implemented these models for their analysis ([36]-[38]). While linear and bi-linear models describe the simplified bond shear-slip behavior, non-linear models capture the bond characteristics obtained from experiments more accurately. One of the widely known non-linear models is Popovics' expression [39], originally developed by Popovics (1973), for the stress-strain relation of concrete. Nakaba et al. (2001) [31] first implemented the expression to describe the shear-slip behavior of FRP debonding, and other authors ([40]-[45]) applied it to their research.

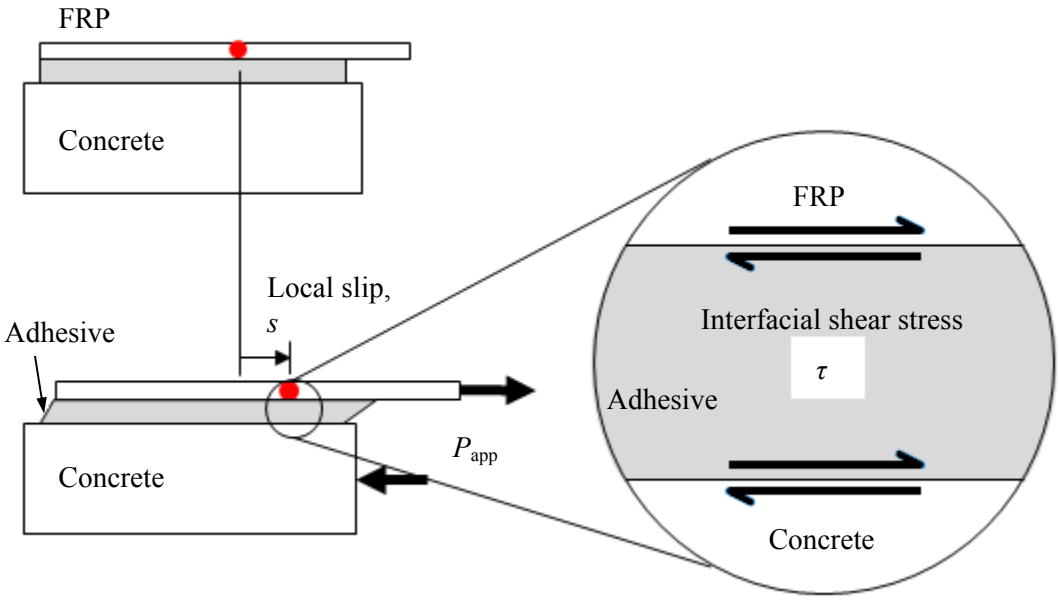

Figure 2.3 Interfacial Shear Stress and FRP Local Slip in Single Pull-off Test

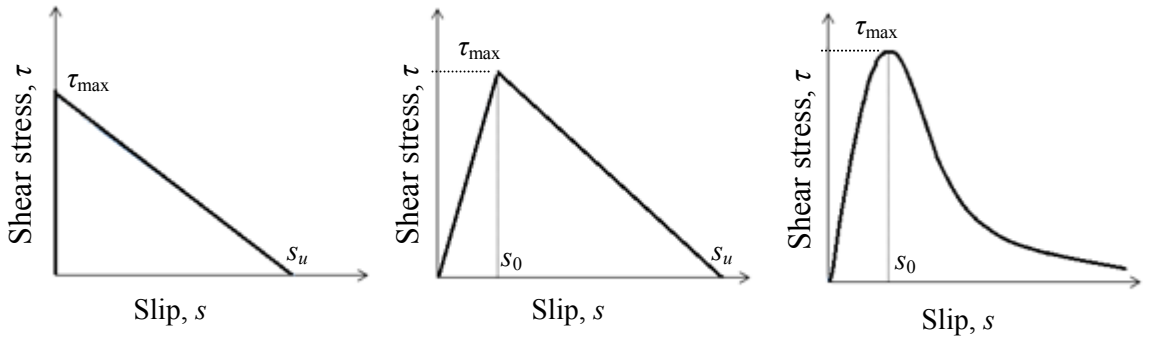

(a) Linear shear-slip curve (b) Bi-linear shear-slip curve (c) Non-linear shear-slip curve

Figure 2.4 Shear-Slip Curve Models

The effective bond length denoted as L_e is a parameter involved in P_{max} prediction in some models. The effective bond length is defined as the minimum bond length where the bond strength can reach to the maximum potential. In other words, with the bond length less than the effective bond length, the bond strength might not reach its maximum, and in the bond system with a longer bond length than L_e, the maximum bond strength does not increase. To determine L_e, authors proposed empirical ([28], [37], [46], and [47]) and theoretical expressions ([38] and [47]).

For analysis on the bond behavior and strength, the interfacial fracture energy, G_f, is implemented and defined as the work done by the interfacial shear stress until the FRP sheet separation. Mathematically, it is obtained by integrating the shear-slip function from 0 to s_u, which is the area under the shear-slip curve. Some researchers examined the relation between compressive strength of concrete substrate f_c' and G_f to determine the expression for G_f ([48]-[54]). Existing research has presented the prediction models of P_{max} as directly proportional to the square root of G_f [50]. To obtain the expression for G_f

theoretically, values for the interfacial maximum shear stress τ_{max} and the corresponding slip s_0 are assessed. Some empirical expressions for τ_{max} and s_0 are derived as a function of f_c'. Instead of using these expressions, constant values were implemented in some studies. In literature, the ultimate slip s_u is less reported compared to s_0 due to the difficulty in measuring s_u accurately during the test. This difficulty is due to a relatively low level of loading on composite specimens where the FRP sheet separation occurs suddenly [55].

2.3 Existing Models

Existing models presented in this section have simple expressions for predicting the maximum transferable load P_{max}. In general, all of the models considered FRP and concrete material properties and neglected adhesive material properties except one model [51]. Some models considered the effect of width configuration of FRP and concrete substrate which is represented as the width ratio of FRP to concrete, b_p/b_c. This ratio is used as a modification factor for P_{max} and L_e. In the coming sections, these models to predict P_{max} are presented.

2.3.1 Holzenkämpfer's Model [36]

Holzenkämpfer investigated the bond strength between steel plates and concrete, applying non-linear fracture mechanics to derive the most widely recognized simple expression for P_{max} as the function of the interfacial fracture energy G_f and FRP tensile stiffness $E_p t_p$. This expression is given by

$$P_{max} = b_p \sqrt{2 G_f E_p t_p} \tag{2.1}$$

where b_p, E_p, and t_p are the width, Young's modulus, and the thickness of FRP, respectively. Many prediction models are based on Equation (2.1). Also, the maximum

interfacial shear stress τ_{max} was expressed by adopting stress transformation based on Mohr-Coulomb as following;

$$\tau_{\max} = \frac{1}{2}\sqrt{f_c' f_t} \tag{2.2}$$

where f_c' and f_t are the concrete compressive strength and tensile strength, respectively.

2.3.2 Neubauer and Rostásy's Model [37]

Holzenkämpfer's model was expanded to predict the strength of composite materials with thin carbon plates bonded to concrete structures. The coefficient k_b and the effective bond length L_e were newly introduced into Equation (2.1), considering interlaminar bond failure in addition to concrete failure. The interfacial fracture energy was expressed as

$$G_f = C_f f_t \tag{2.3}$$

where C_f is reported as 0.202 mm based on his experiment and f_t is found in the CEB-FIP Model Code [56] as

$$f_t = 1.4\left(\frac{f_c' - 8}{10}\right)^{2/3} \tag{2.4}$$

where f_c' is in units of MPa. The P_{max} prediction is expressed as

$$P_{\max} = \begin{cases} 0.64 k_b b_p \sqrt{E_p t_p f_t} & \text{when } L \geq L_e \\ 0.64 k_b b_p \sqrt{E_p t_p f_t}\,\dfrac{L}{L_e}\left(2 - \dfrac{L}{L_e}\right) & \text{when } L < L_e \end{cases} \tag{2.5}$$

where k_b is the width effect coefficient given by

$$k_b = \sqrt{1.125\frac{2 - (b_p/b_c)}{1 + (b_p/400)}}. \tag{2.6}$$

The effective bond length was determined as the following expression;

$$L_e = \sqrt{\frac{E_p t_p}{2 f_t}} \,. \tag{2.7}$$

2.3.3 Brosens' Model [52]

Microscopic analysis was carried out as the extension of the previous work [48] to yield the interfacial fracture energy in terms of concrete tensile strength f_t with coefficients k_b and k_c as

$$G_f = k_b{}^2 k_c{}^2 C_f f_t \tag{2.8}$$

where C_f is an empirically calibrated value as 0.40 through the experimental results. The parameter k_b was related to the width ratio of b_p/b_c and is given by

$$k_b = \sqrt{\frac{k\left(2 - b_p / b_c\right)}{1 + b_p / b_0}} \tag{2.9}$$

where k is an empirical constant determined by experimental calibration as 1.47 mm and b_0 is a parameter representing a reference thickness t_{ref}, which was proposed by Brosens and Van Gemert (1999) [48] to account for the stress influence depth in substrate. The value for t_{ref} was determined to be 2.5 to 3 times the maximum aggregate size, usually resulting in a depth of 40 to 50 mm. The parameter b_0 was expressed as

$$b_0 = \frac{t_{\text{ref}}}{k - 1} \tag{2.10}$$

where t_{ref} = 40 mm. The parameter k_c is used to represent the level of concrete surface preparation condition depending on environmental effect and workmanship in the range of 0.65 to 1.0. With those parameters and constants, the interfacial fracture energy was expressed as

$$G_f = \frac{0.588\left(2 - b_p/b_c\right)}{1 + b_p/85} f_t . \tag{2.11}$$

The expression for $P_{\max}$ is the same as Equation (2.1).

2.3.4 Chen and Teng's Model [45]

In order to obtain a simple and practical model, Chen and Teng used constant values for s_0 and s_u as 0.02 mm and 0.2 mm, respectively. This model includes the width ratio effect of FRP and concrete substrate with the coefficient β_p as shown in the following;

$$\beta_p = \sqrt{\frac{2 - \left(b_p/b_c\right)}{1 + \left(b_p/b_c\right)}} . \tag{2.12}$$

Applying a linear shear-slip model for their analysis, the expression for $P_{\max}$ was obtained as

$$P_{\max} = 0.42 \beta_p \beta_L b_p L_e \sqrt{f_c'} \tag{2.13}$$

where

$$\beta_L = \begin{cases} 1 & \text{when } L \geq L_e \\ \sin\dfrac{\pi L}{2L_e} & \text{when } L < L_e \end{cases} \tag{2.14}$$

$$L_e = \sqrt{\frac{E_p t_p}{\sqrt{f_c'}}} . \tag{2.15}$$

2.3.5 Dai et al.'s Model [51]

Based on Equation (2.1), the bond width effect was introduced into the expression as Δb_p, which was originally proposed by Sato et al. (2000) [46]. The expression for $P_{\max}$ was obtained as

$$P_{\max} = \left(b_p + 2\Delta b_p\right)\sqrt{2G_f E_p t_p} \tag{2.16}$$

where Δb_p can be taken as 3.7 mm when the bond width exceeds 100 mm. Considering adhesive effect on bond strength, the interfacial fracture energy was determined implementing adhesive material properties as parameters. From the experimental results and regression analysis, the expression for G_f was obtained as

$$G_f = 0.446\left(\frac{G_a}{t_a}\right)^{-0.352} f_c'^{0.236}\left(E_p t_p\right)^{0.023} \tag{2.17}$$

where G_a and t_a are shear modulus (GPa) and the thickness (mm) of the adhesive material, respectively.

2.3.6 Lu et al.'s Model [50]

Lu et al.'s model was based on meso-scale finite element analysis simulating FRP debonding to determine values for different coefficients. The expression for $P_{\max}$ is given by

$$P_{\max} = \beta_l b_p \sqrt{2G_f E_p t_p} \tag{2.18}$$

where β_l was originally implemented in Chen and Teng's model [45]. The interfacial fracture energy was determined with the simplified expression as

$$G_f = 0.308\beta_w^{\,2}\sqrt{f_t} \tag{2.19}$$

$$\beta_w = \sqrt{\frac{2.25 - \left(b_p/b_c\right)}{1.25 + \left(b_p/b_c\right)}} \tag{2.20}$$

where f_t is determined according to the Chinese code for the design of concrete structures as [57]

$$f_t = 0.395 f_{cu}^{\,0.55} \tag{2.21}$$

$$f_{cu} = \frac{f_c'}{0.76} \tag{2.22}$$

where f_{cu} is the cube compressive strength of concrete. For the bond behavior, an analytical solution was developed and the effective bond length was determined as

$$L_e = a + \frac{1}{2\lambda_1} \ln \frac{\lambda_1 + \lambda_2 \tan(a\lambda_2)}{\lambda_1 - \lambda_2 \tan(a\lambda_2)} \tag{2.23}$$

$$a = \frac{1}{\lambda_1} \arcsin\left(0.99 \sqrt{\frac{s_u - s_0}{s_u}} \right) \tag{2.24}$$

$$\lambda_1 = \sqrt{\frac{\tau_{\max}}{s_0 E_p t_p}} \tag{2.25a}$$

$$\lambda_2 = \sqrt{\frac{\tau_{\max}}{(s_u - s_0) E_p t_p}} \tag{2.25b}$$

where

$$\tau_{\max} = 1.50 \beta_w f_t \tag{2.26}$$

$$s_0 = 0.0195 \beta_w f_t \tag{2.27}$$

$$s_u = \frac{2G_f}{\tau_{\max}} . \tag{2.28}$$

2.3.7 Karbhari et al.'s Model [54]

Karbhari et al. extended Nakaba et al.'s model [31] to provide the expression for G_f in a simple form as a function of concrete compressive strength f_c'. The expression is given by

$$G_f = 0.644 f_c'^{0.19} . \tag{2.29}$$

The expression for $P_{\max}$ is the same as Equation (2.1).

CHAPTER III

THEORETICAL DERIVATION FOR FRP BOND STRENGTH

3.1 Critical Stress State Criterion for Debonding in a Single Pull-off Test

In this study, to predict the bond behavior and strength, the debonding mechanism of FRP to concrete structure is examined based on a single pull-off test configuration. The FRP debonding is considered as a fracture process in concrete substrate due to the critical local stress at a certain depth. The applied load P_{app} at the end of the FRP strip is transmitted into concrete substrate through an adhesive layer as the interfacial shear stress represented by a distribution function of $\tau(x)$. As the level of the applied load increases, the interfacial shear stress increases to eventually reach its maximum value of τ_{max}. This τ_{max} induces the critical stress state in substrate and initiates concrete failure.

In general, concrete substrate failure at a few millimeters below the adhesive−concrete interface is agreed as the major factor for debonding. An experiment by Yao et al. (2005) confirmed that a thin concrete layer with 1 to 5 mm thickness was observed on the most debonded FRP strips [58]. Brosens and Van Gemert (1999) and Brosens (2001) considered this layer in substrate as the reference distance or the epoxy−mortar layer. In addition to the thickness of the adhesive layer, the thickness of

the layer in substrate affects the FRP local slip and the bond strength. This fracture depth was denoted as t_{ref} in the expression for the maximum transferable load. They mentioned to a fracture depth of 2.5 to 3 times the maximum aggregate size in concrete ([48] and [52]). Assuming such concrete failure, a criterion for debonding initiation can be related to concrete tensile strength. Considering a point at a depth t and at a distance d away from the loading bond end, the stress state in concrete substrate $\sigma_{e,d}$ should not exceed a limit bond stress as shown below;

$$\sigma_{e,d} \leq f_b \tag{3.1}$$

where f_b is the limit bond stress in concrete substrate for FRP debonding. Direct pull-out test on concrete shown in Figure 3.1 illustrates Equation (3.1). An illustrative sketch of a direct pull-out test and the sample of experimental result are shown in Figure 3.1 (a) and Figure 3.1 (b), respectively. Thus, the limit bond stress f_b can be assumed as concrete tensile strength f_t expressed as $0.56f'^{0.5}_c$ in units of MPa [59].

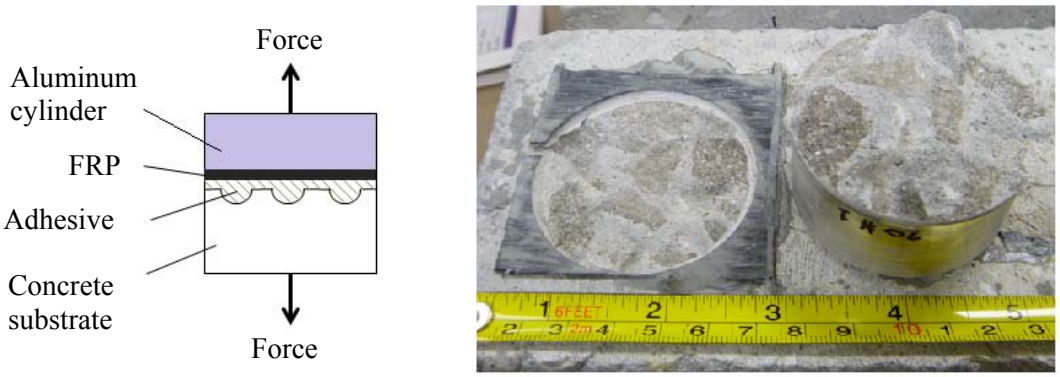

(a) Sketch of Pull-out Test

(b) Cylinder and Substrate of Pull-out Test

Figure 3.1 Direct Pull-Out Test

From the observation on cylinders during the pull-out test, not only cement but aggregate particles are pulled out of concrete substrate. The amount of concrete attached to cylinders indicates concrete fracture initiates much deeper in the direct pull-out test than that of a single pull-off test where a thin concrete layer is attached to FRP. This infers that concrete tensile strength is not fully utilized in a single pull-off test. Also, the effects of surface condition of concrete substrate, such as roughness and exposed aggregate amount, can be factors for the bond strength. Considering these factors, modified concrete tensile strength for FRP debonding is to be introduced in this study. This modification is implemented as the strength factor α in units of %. Applying the strength factor, Equation (3.1) can be revised as

$$\sigma_{e,d} \le \alpha f_t = \alpha\left(0.56\sqrt{f_c'}\right). \tag{3.2}$$

3.2 Stress State in Concrete Substrate Induced by Interfacial Shear Stress

From the elasticity theory, the stress state σ_e, on an element in the material subjected to a horizontal surface load can be expressed as [60]

$$\sigma_e = \frac{2H}{\pi r}\sin\theta \tag{3.3}$$

where H is the horizontal force on the material surface; r is the radial distance from the loading point; θ is the angle measured from the vertical line at the loading point to the radial line in clockwise positive as shown in Figure 3.2.

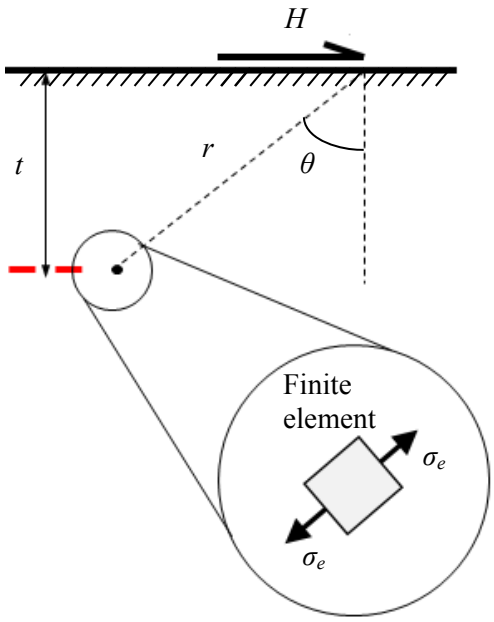

Figure 3.2 Stress State in Finite Element Induced by Horizontal Surface Load

For the validity of the application of 2-D mechanics of materials and the elasticity theory, it is assumed that the FRP sheet is subjected to only axial forces and the shear stress in a plane strain condition. During a single pull-off test, the expedient concentrated horizontal load at a point is expressed as $\tau(x)dx$. This leads to a differential stress state $d\sigma_e$ acting perpendicularly to the plane of a square finite element. The differential stress on the element, $d\sigma_e$, induced by the load at any point along the bond length can be given by

$$d\sigma_e = \frac{\tau(x)dx}{\pi t}\sin 2\theta \tag{3.4}$$

where t is the depth of the considered element embedded in concrete. It is also denoted as the fracture depth. In this study, if the differential stress is tensile, it is considered positive

in Equation (3.4). Since consecutive horizontal loads at each loading point along the bond length are considered, infinite numbers of differential stresses are superimposed on the same element. For the critical stress state in tension, all differential stresses are transformed to a single plane using the Mohr's circle, denoted as the critical plane [61]. On an element at a distance d from the loaded end and at a depth t, the critical normal stress $\sigma_{e,d}$ is expressed as

$$\sigma_{e,d} = \int_0^L \frac{\tau(x)}{2\pi t}(1+\cos 2\theta_1)\sin 2\theta_2 dx \tag{3.5}$$

where θ_1 and θ_2 are the transformation angle and the position angle, respectively. The expression for θ_2 is as $\tan^{-1}\{x-(L-d)\}/t$. The integrand in Equation (3.5) represents the differential stress state transformed onto the critical plane which is at the angle $\theta = \pi/4$ from Equation (3.4) or at the angle $\theta_3 = \tan^{-1}(d/t)$ when the plane with $\theta = \pi/4$ is not defined (Figure 3.3). The transformation angle θ_1 is given by

$$\theta_1 = \begin{cases} \theta_2 - \theta_3, & d < t \\ \theta_2 - \frac{\pi}{4}, & d \geq t \end{cases}. \tag{3.6}$$

If $d < t$, where the considered element is relatively close to the loaded end, the critical plane is at the angle θ_3 (Figure 3.3(a)). If the considered element is in the range of $d \geq t$, each differential stress is transformed on the plane with the angle $\pi/4$ (Figure 3.3(b)). Equation (3.5) is substituted into Equation (3.2) to relate the critical stress criterion to the interfacial shear stress distribution, and the criterion is expressed as

$$\int_0^L \frac{\tau(x)}{2\pi t}(1+\cos 2\theta_1)\sin 2\theta_2 dx \leq \alpha\left(0.56\sqrt{f'_c}\right). \tag{3.7}$$

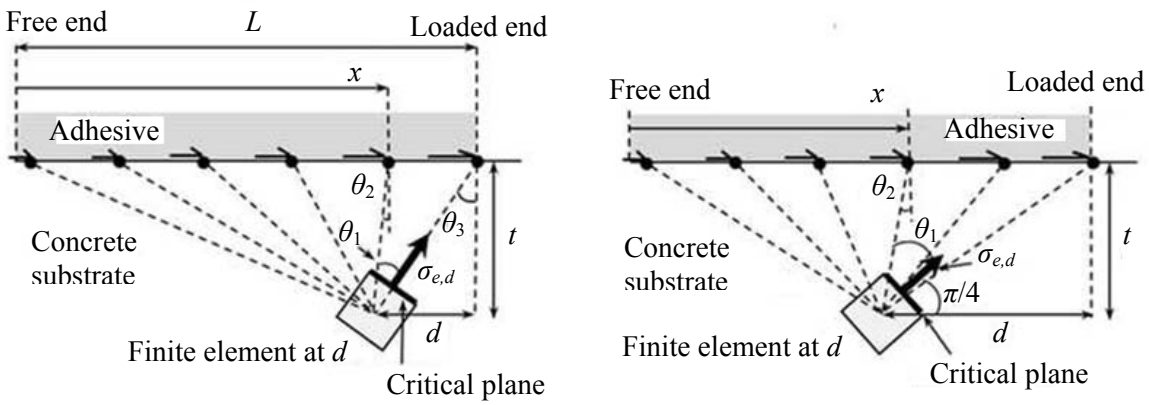

Figure 3.3 Transformed Stress on Critical Plane of Concrete Element

3.3 Non-linear Bond Shear-Slip Model: Popovics' Expression

The importance of non-linear shear-slip models for the FRP bond joint is to capture the softening characteristics after the shear stress peak. The Popovics' expression [39] was implemented as the bond shear-slip curve model as a function of the maximum interfacial shear stress, τ_{max}, the corresponding local slip, s_0, and a parameter n. The curve is expressed as follows:

$$\tau(s) = \tau_{max} \frac{s}{s_0} \left\{ \frac{n}{(n-1) + (s/s_0)^n} \right\}. \tag{3.8}$$

With different values of the parameter n, corresponding curves appear almost linear until the peak value followed by softening branches at each descent degree dependent on n as illustrated in Figure 3.4. The interfacial fracture energy G_f can be determined by

following the definition integrating Equation (3.8) from 0 to ∞ [54]. The expression for G_f is given by

$$G_f = \frac{\tau_{\max}}{s_0}\int_0^{\infty} s\left\{\frac{n}{(n-1)+(s/s_0)^n}\right\}ds\,. \tag{3.9}$$

However, the local slip s never reaches infinity in reality, and the upper limit in Equation (3.9) can be replaced by the ultimate local slip s_u with the experimentally calibrated value of 0.42 mm ([55] and [62]). For simplification and compatibility, the value for n is considered as 3 [31], and Equation (3.9) becomes

$$G_f = \frac{3\tau_{\max}}{s_0}\int_0^{0.42} s\left\{\frac{1}{2+(s/s_0)^3}\right\}ds\,. \tag{3.10}$$

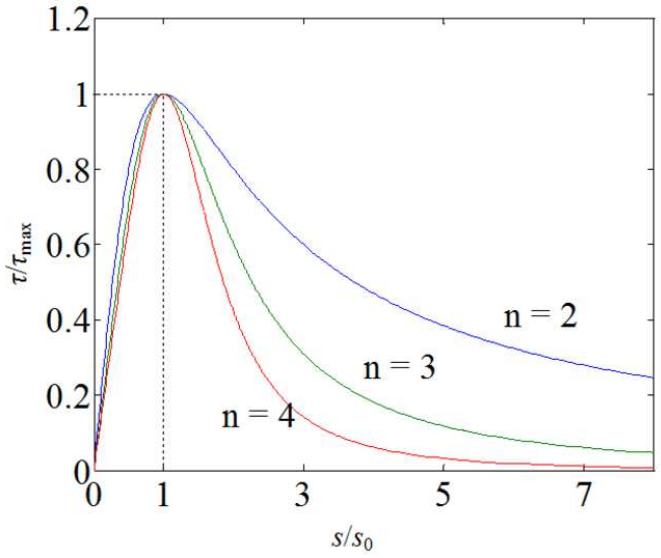

Figure 3.4 Interfacial Shear Stress vs. FRP Local Slip by Popovics' Expression

3.4 Development of Analytical Solution

The expression for the interfacial shear stress distribution $\tau(x)$ needs to be derived for the application of the critical stress criterion (Equation (3.7)) for predicting the bond strength. Also, values for the maximum interfacial shear stress τ_{max} and the corresponding local slip s_0 are required for predicting the interfacial fracture energy (Equation (3.10)). For determining these expressions and values, the fundamental mechanics of materials and the elasticity theory are used to develop an analytical solution describing the bond behavior. For a simple mechanical constitutive equation, elastic behavior and perfect bond are assumed on the FRP to concrete bond joint until the interfacial shear stress τ reached its peak τ_{max}.

The local slip of the FRP strip is simply considered as the axial elongation due to the tensile stress in the strip. At the interface to the FRP strip, the adhesive layer deforms due to the interfacial shear stress (Figure 3.5). Considering a small segment at the bond interface, the axial elongation due to the axial stress in the adhesive layer contributes the adhesive displacement to match the FRP local slip as shown in Figure 3.5. The concrete substrate deformation is neglected since it is relatively small. Considering the deformation of the adhesive layer, the FRP local slip is expressed as

$$\frac{ds}{dx} = \frac{dl}{dx} + \frac{d\delta}{dx} \tag{3.11}$$

where s is the local slip; l is the shear deformation; δ is the axial elongation due to the axial stress in the adhesive layer at the interface to FRP. Based on mechanics of materials, stress-strain relations for FRP and adhesive are defined as

$$\frac{ds}{dx} = \frac{\sigma_p(x)}{E_p} \tag{3.12}$$

$$\tau = G_a \gamma_a = G_a \frac{l}{t_a} \tag{3.13}$$

$$\frac{d\delta}{dx} = \frac{\sigma_a(x)}{E_a} \tag{3.14}$$

where σ_p is the axial tensile stress in the FRP strip expressed as $\sigma_p(x) = P_{app}(x)/b_p t_p$ and σ_a is the interfacial axial stress in the adhesive layer. From the axial force equilibrium state, the interfacial shear stress can be related to the axial tensile stress σ_p in FRP. The equilibrium expression is shown below [63]:

$$\tau(x) = t_p \frac{d\sigma_p}{dx}. \tag{3.15}$$

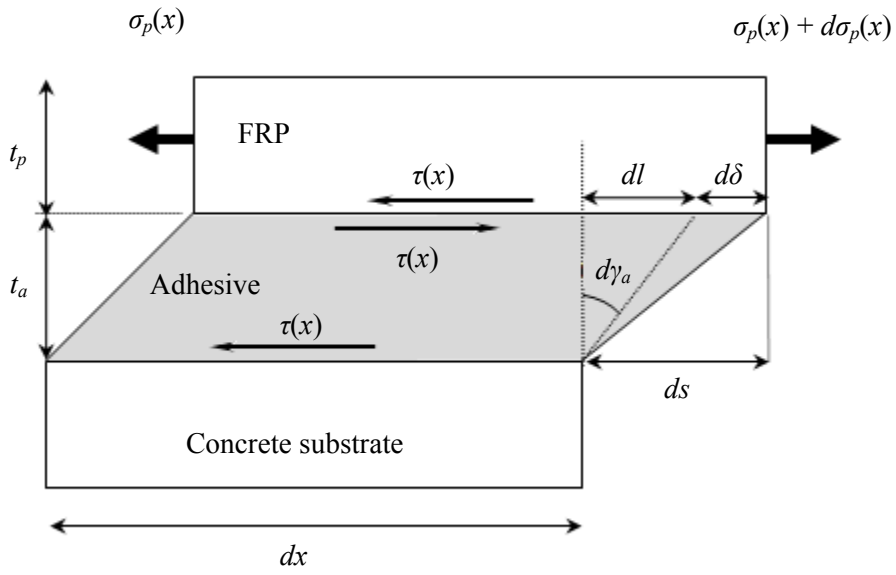

Figure 3.5 Deformation in Small Segment of FRP Bond Joint

It is assumed that the stress state on a finite element in the adhesive layer is induced by the interfacial shear stress subjected to the interface of the adhesive layer to the FRP strip. For simplification, the differential stress state is obtained on the boundary line between two small consecutive segments in the adhesive layer by superimposing two differential stress states. At the middle points 1 and 2 on each adhesive segment surface, the corresponding horizontal surface loads are defined as τdx and $(\tau + d\tau)\ dx$ (Figure 3.6). Each differential stress state induced by horizontal surface loads is denoted as $d\sigma_1$ and $d\sigma_2$, respectively, and expressed as the function of angle θ by applying the elasticity theory as shown earlier in this chapter. By superimposing these two differential stresses at the middle point between 1 and 2 on the interface to the FRP strip, the expression for the differential stress $d\sigma_a$ is obtained as

$$d\sigma_a = \frac{4d\tau}{\pi}. \tag{3.16}$$

The fundamental assumption on the interfacial shear stress is made that the first peak stress occurs at the loaded end and it shifts towards adjacent points. Substituting Equations (3.12) to (3.16) into Equation (3.11) and differentiating it, the governing equation in terms of the variable τ is yielded as following with coefficients A and B:

$$\frac{d^2\tau}{dx^2} + A\frac{d\tau}{dx} - B\tau = 0 \tag{3.17}$$

where

$$A = \frac{4G_a}{\pi E_a t_a} \tag{3.18}$$

$$B = \frac{G_a}{E_p t_p t_a}. \tag{3.19}$$

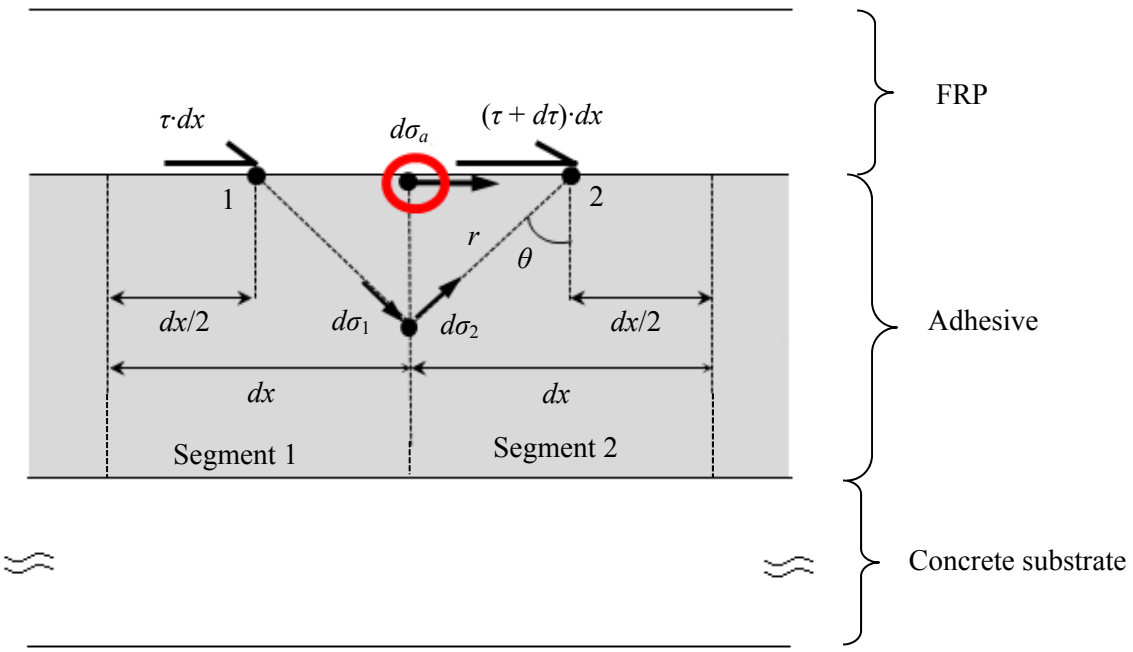

Figure 3.6 Stress State in Small Segment of Adhesive Layer at Interface to FRP

For the solution of the second order differential equation (Equation (3.17)), the boundary conditions at $x = 0$ and L are applied. The free end experiences no slip or stress yielding $\tau(0) = 0$. With the assumption that no stress dissipation or loss arises through the unbounded part of the FRP strip, the loading end condition is obtained as $\sigma_p(L) = P_{app}/(b_p t_p)$, where P_{app} is the actual load level applied at the end of the FRP strip. The applied load level corresponding to τ_{max} is denoted as $P_{app\_\tau max}$. With these boundary conditions, solving Equation (3.17) yields the expression for the interfacial shear stress distribution along the bond length as

$$\tau(x) = C(P_{app})D(x) \tag{3.20}$$

where

$$C\left(P_{\text{app}}\right)=\frac{P_{\text{app}}}{b_p}\left(\frac{e^{\lambda_1 L}-1}{\lambda_1}-\frac{e^{\lambda_2 L}-1}{\lambda_2}\right)^{-1} \tag{3.21}$$

$$D(x)=e^{\lambda_1 x}-e^{\lambda_2 x} \tag{3.22}$$

where λ_1 and λ_2 are positive and negative roots of the characteristic equation, respectively. From Equation (3.11) with the substitution of Equations (3.20) to (3.22), the local slip expression can be derived as

$$s(x)=C\left(P_{\text{app}}\right)\left\{\frac{t_a}{G_a}D(x)+\frac{4}{\pi E_a}E(x)\right\} \tag{3.23}$$

where

$$E(x)=\frac{e^{\lambda_1 x}-1}{\lambda_1}-\frac{e^{\lambda_2 x}-1}{\lambda_2}. \tag{3.24}$$

The maximum interfacial shear stress $\tau_{\max}$ at the loaded end $x = L$ is expressed by using Equations (3.20) to (3.22) with the load level of $P_{\text{app\_}\tau\max}$ as

$$\tau_{\max}=\tau(L)=C\left(P_{\text{app\_}\tau\max}\right)D(L). \tag{3.25}$$

From Equation (3.25), $P_{\text{app\_}\tau\max}$ is expressed in terms of $\tau_{\max}$ and substituted into Equations (3.20) and Equations (3.23) at $x = L$ to derive the expressions for the interfacial shear distribution $\tau(x)$ and the corresponding slip s_0 as followings:

$$\tau(x)\cong\tau_{\max}\frac{D(x)}{e^{\lambda_1 L}} \tag{3.26}$$

$$s_0\cong\tau_{\max}\left(\frac{t_a}{G_a}+\frac{4}{\lambda_1\pi E_a}\right). \tag{3.27}$$

CHAPTER IV

NUMERICAL COMPARISONS

4.1 Numerical Analysis with Proposed Criterion and Analytical Solution

The proposed criterion and expression were applied for a given set of material properties of the FRP bond system to predict the maximum transferable load in a single pull-off test. A MATLAB program was written to perform the necessary calculations for the prediction. An experimental data set provided by Dai et al. (2005) [51] were used as input parameters including adhesive properties for analysis. Thicknesses of the FRP strip and the adhesive layer are shown in Table 4.1. Other necessary material properties are given by G_a = 873.19 MPa, E_a = 2410 MPa, f_c' = 35 MPa, E_p = 230,000 MPa, L = 330 mm, and b_p = 100 mm. By applying the expression for $\tau(x)$ from Equations (3.26), the distribution of the ratio of $\sigma_{e,d}/\tau_{max}$ along the bond length for each specimen with the maximum values of the ratio is obtained. From the proposed criterion (Equation (3.2)), τ_{max} is simply determined by dividing αf_t by the maximum value of $\sigma_{e,d}/\tau_{max}$. The P_{max} prediction procedure proposed in this study is illustrated as a flowchart in Figure 4.1.

Table 4.1 Thickness of the Adhesives and FRP from Dai et al. (2005) [51]

Specimen ID	Thickness	
	Adhesive, t_a	FRP, t_p
	mm	mm
CR1L1-a	0.9002	0.11
CR1L1-b	0.7660	0.11
CR1L2-a	0.9002	0.22
CR1L2-b	0.7660	0.22
CR1L3-a	0.9002	0.33
CR1L3-b	0.7660	0.33

C = carbon fiber; R1 = epoxy type; L1-L3 = number of FRP plies; -a & -b = different adhesive thickness.

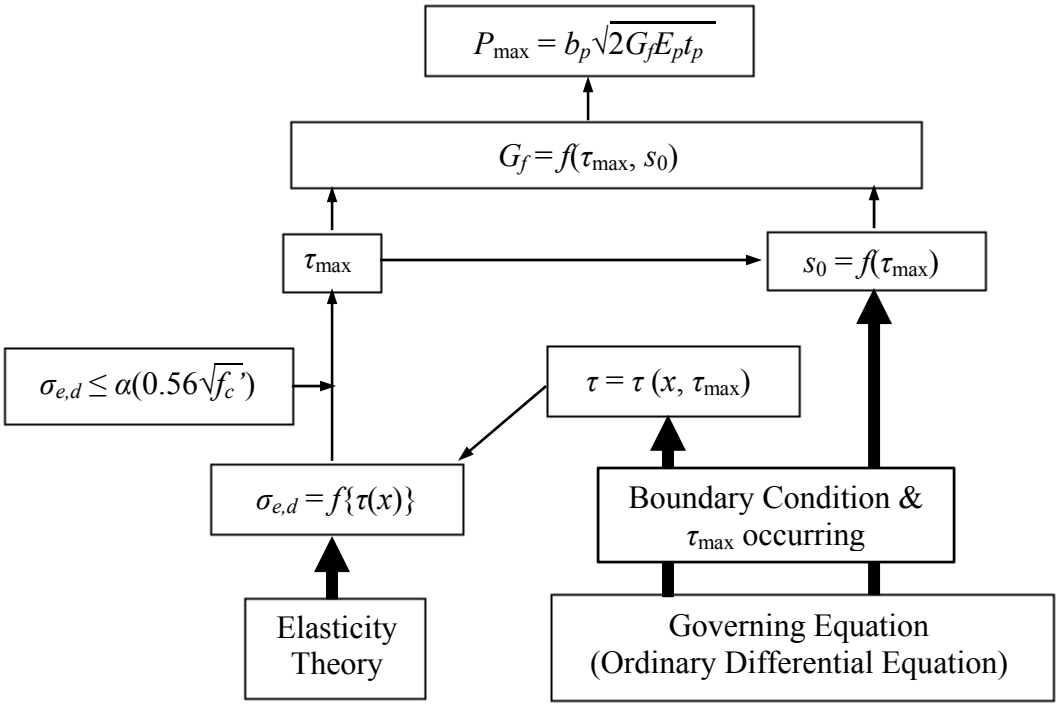

Figure 4.1 Flowchart of Process for Predicting Maximum Transferable Load

4.2 Parameter Study

Parametric study on the effect of the fracture depth t was performed for specimen CR1L1-a from Dai et al.'s experiment (2005) [51]. The strength factor α was set as 125% to emphasize the effect of t. The relation between the predicted P_{max} and the depth t was plotted as shown in Figure 4.2. The minimum value for predicted P_{max} was obtained with the fracture depth t = 0.13 mm. The predicted P_{max} increased linearly with t deeper than 0.13 mm, whereas the curve was asymptotically increasing to infinity with t < 0.13 mm. The fracture depth t as 0.0552 mm or 1.08 mm was obtained matching the predicted P_{max} to the experimental result P_{max} = 23.4 kN for specimen CR1L1-a. Since fracture in substrate occurs at a few millimeters below the adhesive□concrete interface, t = 1.08 mm was more realistic and consistent with the experimental results.

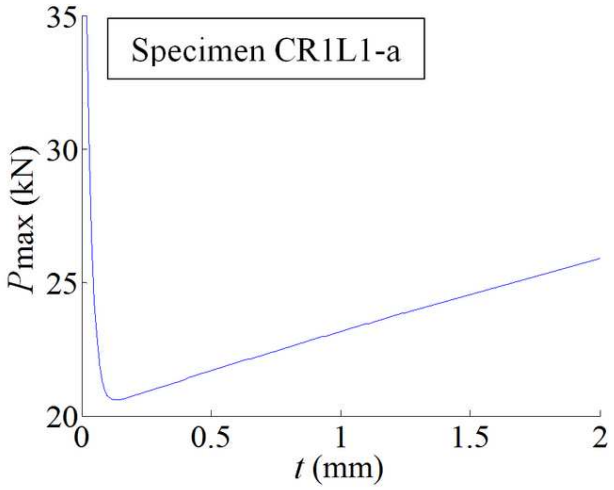

Figure 4.2 Predicted P_{max} vs. Fracture Depth for Specimen CR1L1-a

The distribution of the ratio $\sigma_{e,d}/\tau_{max}$ shown in Figure 4.3 indicates that the stress state on a concrete element reaches the maximum value at a few millimeters away from the loaded end and linearly descends to nearly zero at the free end. This captures the bond characteristics claimed in literature based on experimental observations. The predicted values for specimen CR1L1-a with the different fracture depth t are shown in Table 4.2. These values are obtained from the plot (Figure 4.2). For predicting the bond strength of other specimens from the experiment carried out by Dai et al. (2005) [51], the fracture depth t = 1.0 mm was applied, and the result is shown in Table 4.3. The predicted and the experimental values are in good agreement for a single ply and double plies of FRP specimens. However, for three-ply FRP specimens, the prediction overestimates the bond strength. This might be due to experimental uncertainties. With the increase in the number of FRP plies, more thickness is to be pinched and pulled by the testing machine. A slip is more likely to happen between FRP and the grips or between plies.

Table 4.2 Predicted Values with Different t for Specimen CR1L1-a

t	Max $\sigma_{e,d}/\tau_{max}$	d	τ_{max}	s_0	P_{max}
mm		mm	MPa	mm	kN
0.0552	0.5885	8.3	7.037	0.063	23.40
0.5	0.6400	8.4	6.471	0.05	21.68
1.08	0.5881	9.8	7.042	0.063	23.42
1.5	0.5578	10.8	7.424	0.067	24.56
2.0	0.5257	11.8	7.878	0.071	25.91

Table 4.3 Predicted Values with t = 1.0 mm for Specimens from Dai et al. (2005) [51]

Specimen ID	Predicted load P_{pred}	Experiment load P_{exp} Dai et al [51]	Ratio P_{exp}/P_{pred}
	kN	kN	
CR1L1-a	23.16	23.4	1.010
CR1L1-b	22.86	23.1	1.010
CR1L1-b	22.86	24.9	1.089
CR1L2-a	38.65	33.5	0.867
CR1L2-b	38.37	39.3	1.024
CR1L3-a	53.71	42.9	0.799
CR1L3-b	53.48	38.4	0.718
CR1L3-b	53.48	36.9	0.690

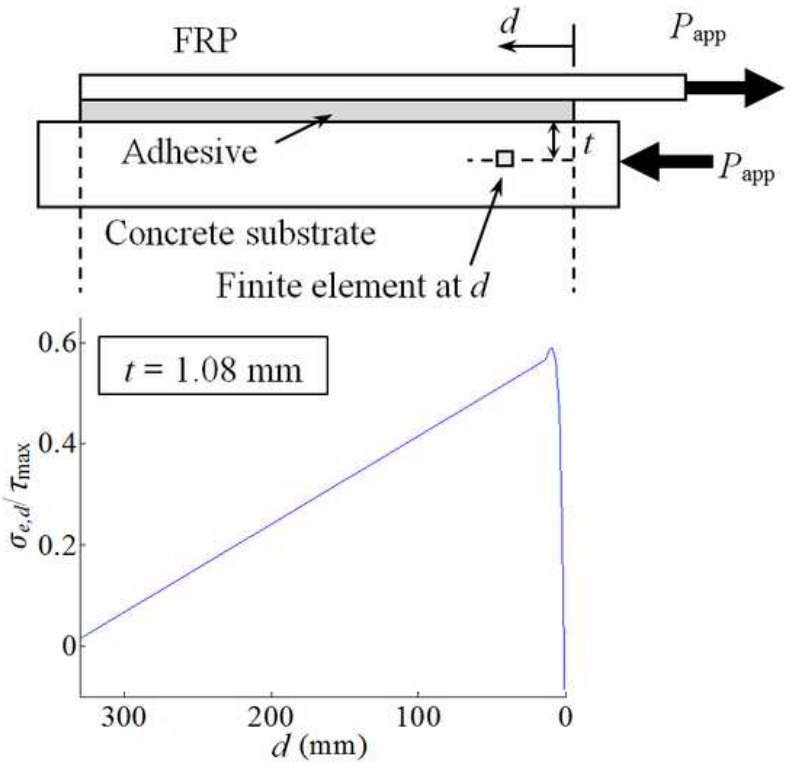

Figure 4.3 Distribution of $\sigma_{e,d}/\tau_{max}$ along Bond Length for Specimen CR1L1-a

4.3 Interfacial Fracture Energy Prediction

Using the experimental data from Dai et al. (2005) [51], the prediction for G_f from the proposed expression was compared with G_f obtained experimentally and with the prediction from existing empirical models. The model by Ueda et al. (2003) [34] considered adhesive material properties and thickness as parameters and derived the expression for G_f as $0.446(G_a/t_a)^{-0.352}f_c'^{0.236}(E_pt_p)^{0.023}$ in Equation (2.17). Karbhari et al. (2006) [54] implemented the non-linear Popovics' expression for the shear-slip relation with n as 3, and obtained the expression for G_f in a simple form as $G_f \approx 0.184\tau_{max} \approx 0.644f_c'^{0.19}$ in Equation (2.29). Lu et al. (2005) [50] considered the width ratio b_p/b_c in the expression for G_f as $0.308\beta_w^2 f_t^{0.5}$ where $\beta_w = \{(2.25 - b_p/b_c)/(1.25 + b_p/b_c)\}^{0.5}$ (Equation (2.19) and (2.20)). The comparison result is shown in Table 4.4. In the result, G_f values from existing models ([50] and [54]) were constant for all the specimens since those expressions are simply proportional to concrete compressive strength. In contrast, Ueda et al.'s model [34] showed a variation in G_f value corresponding to different adhesive properties. By predicting corresponding values for each specimen, the proposed prediction showed good agreement with experimental G_f.

Table 4.4 Predicted G_f from Proposed Expression and Existing Models

Specimen ID	G_f				
	Experiment Dai et al. (2006) [51]	Proposed	Ueda et al. (2003) [34]	Lu et al. (2005) [50]	Karbhari et al. (2006) [54]
	N/mm	N/mm	N/mm	N/mm	N/mm
CR1L1-a	1.082	1.060	0.116	1.265	0.730
CR1L1-b	1.139	1.033	0.109	1.265	0.730
CR1L2-a	1.109	1.476	0.118	1.265	0.730
CR1L2-b	1.526	1.455	0.111	1.265	0.730
CR1L3-a	1.561	1.900	0.119	1.265	0.730
CR1L3-b	1.662	1.884	0.112	1.265	0.730

CHAPTER IV

EXPERIMENTAL PROGRAM

5.1 Test Method

A single pull-off test was conducted for externally bonded FRP reinforced concrete. The load was applied to the bonded FRP strip under displacement controlled until failure. The composite material consisted of concrete substrate with a dimension of 80 mm width × 350 mm length × 100 mm thickness and a FRP strip of 40 mm width × 340 mm length. The thickness of the adhesive layer varied for each specimen. For analyzing the effect of material properties, different compressive strength concrete and two types of adhesive materials were used.

5.2 Material Properties

5.2.1 Concrete Substrate

The concrete substrate dimension was 100×80×350 mm, and a surface of 80×350 mm was treated to bond FRP. To investigate the effect of substrate strength on the bond strength, five different concrete mix designs were used aiming at compressive strength f_c' = 20, 40, 70 MPa as the first set. For the second set, 20 and 40 MPa compressive strength were prepared. The concrete mix contained Type I Portland cement, water, coarse

aggregate (gravel) with maximum nominal size of ¾ in., and fine aggregate (beach sand). Each mix was designed by following concrete mix design texts ([64] and [65]). Considering the water content and the absorption of aggregates, the water adjustment was done on the original amount determined by the water cement ratio in manuals. The concrete mixes were poured into plywood forms. Mixes were adequately consolidated by using the vibrator and a tapping rod. Three cylinders (3×6 in.) from the same concrete mix batch were used to test concrete compressive strength. After pouring, the top of forms and cylinders with fresh concrete were covered with a polyethylene sheet and caps for about 3 days before demolding. Concrete blocks and cylinders were demolded and submerged into water at room temperature for 28 days for curing. After curing, they were taken out to dry until testing. Each concrete mix proportions are provided in Table 5.1.

Table 5.1 Concrete Mix Proportions

Designed strength	20 MPa	40 MPa	70 MPa	20 MPa	40 MPa
	1st Set	1st Set	1st Set	2nd Set	2nd Set
	Kg/m^3	Kg/m^3	Kg/m^3	Kg/m^3	Kg/m^3
Cement	347	435	639	347	435
Water	216	182	178	216	182
Coarse Aggregate	986	1001	1001	986	1001
Fine Aggregate	739	739	589	739	739

To evaluate concrete strength for each mix, a cylinder compressive test was conducted following the standard test method. The test set-up and the machinery are shown in

Figure 5.1. The average compressive strength for each mix was determined as shown in Table 5.2. It is noted that compressive strength values obtained from the test were adjusted with division by 1.08 since compressive strength of 3×6 in. test cylinders are usually higher than those for 6×12 in. standard cylinders by 8% [66].

Figure 5.1 Cylinder Compressive Test Setup

Table 5.2 Compressive Strength of Concrete Mix

Designed strength	20 MPa	40 MPa	70 MPa	20 MPa	40 MPa
	1st Set	1st Set	1st Set	2nd Set	2nd Set
Compressive Strength f_c' (MPa)	23.0	30.8	74.5	28.2	39.1

5.2.2 Carbon Fiber Sheet

The unidirectional carbon fiber sheet used in this study was commercially available, SikaWrap Hex 103C (Sika) and material properties of the fiber are provided by the company as shown in Table 5.3.

Table 5.3 Carbon Fiber Properties of SikaWrap Hex 103C

Carbon fiber SikaWrap Hex 103C	Metric	English
Tensile strength	3,793 MPa	550 ksi
Tensile modulus	234.5 GPa	34 Msi
Elongation	1.5 %	1.5 %
Density	1.8 g/cm^3	0.065 lbs/in.^{3}

Carbon fiber is fabricated unidirectional with thin string woven in transverse direction bundling carbon fibers together (Figure 5.2). The thickness of the sheet was measured as 0.55 mm.

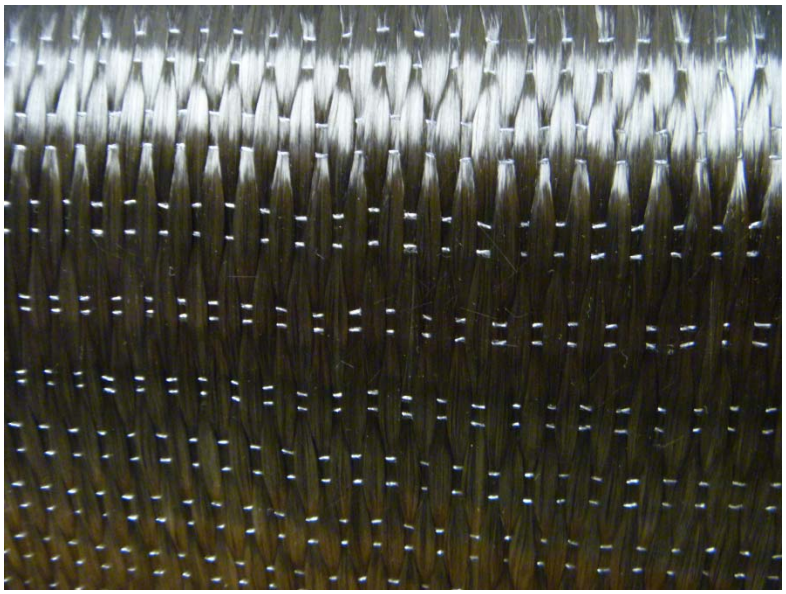

Figure 5.2 Carbon Fiber Sheet (SikaWrap Hex 103C)

5.2.3 Epoxy Resin

Two types of commercially available epoxy resins, Sikadur 301 (Sika) and Quakebond J300SR (QuakeWrap) (Figure 5.3 and 5.4), were used as impregnation and adhesive material embedding carbon fiber in matrix and bonding the FRP strip to concrete substrate. Both epoxy resins are provided in forms of two components: A and B. They were prepared by mixing components at a certain ratio according to user instructions provided by the manufactures. For Sikadur 301, the mix ratio A:B = 3:1 by volume is specified, and the ratio of 2:1 is for Quakebond J300SR. Material mechanical properties are shown in Table 5.4 provided by the manufactures.

Figure 5.3 Sikadur 301 (Adhesive Material)

Figure 5.4 Quakebond J300SR (Adhesive Material)

Table 5.4 Epoxy Resin Properties of Sikadur 301 and Quakebond J300SR

Epoxy properties	Sikadur 301	Quakebond J300SR
Tensile strength (ASTM D-638) 7 days	52.0 MPa (8,000 psi)	49.3 MPa (7,150 psi)
Tensile modulus	2,000 MPa (290 ksi)	1,995 MPa (289.3 ksi)
Elongation	3.5%	NA
Compressive strength (ASTM D-695) 7 days	96.0 MPa (13,900 psi)	65.4 MPa (9,490 psi)
Compressive modulus	1,725 MPa (250 ksi)	3,250 MPa (472 ksi)

5.2.4 CFRP Lamina

As the composite material consisting of a unidirectional carbon fiber sheet and epoxy resin, properties of FRP were obtained with a simple tensile coupon test. The carbon fiber sheet (SikaWrap Hex 103C) was cut into a piece of 20×250 mm stripe with the fiber direction along longer sides, impregnated with epoxy resin, and cured for 7 days at room temperature before specimens were tested. Two types of epoxy resins were used, and for each type of FRP, 3 stripes were assembled. During the impregnating process, steel plates were attached at both ends of the stripe for the proper grip during the tensile test. After curing for 7 days, a strain gauge was attached at the center of each FRP stripe with the specific bond, M-Bond 200 (Vishay Micro-Measurements). The illustrative coupon specimen and its dimensions are schematically shown in Figure 5.5.

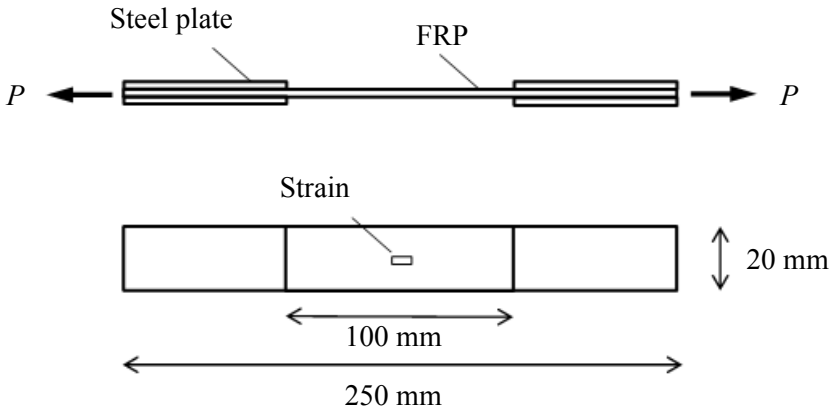

Figure 5.5 FRP Strip for Coupon Test with Side and Plan Views

For the tensile coupon test, an electrical MTS tensile machine was used equipped with manual grips at both actuator and base. The FRP coupon specimen was set on grips as shown in Figure 5.6. As applying tensile load changed, the corresponding strains at the center of the strips in the fiber direction were acquainted and recorded with the data acquisition software. The head speed was set as displacement controlled at the rate of 1 mm/min following the strain measurement standard. The tensile Young's modulus E_p for each FRP was obtained from the data of stress-strain relation. Average values of Young's moduli are shown in Table 5.5 as well as the thickness of the original carbon fiber sheet.

Figure 5.6 FRP Coupon Strip Set on MTS Tensile Machine

Table 5.5 Young's Modulus of FRP and Thickness of Carbon Fiber Sheet

FRP (Fiber: SikaWrap Hex 103C)	Sikadur 301	Quakebond J300SR
Tensile modulus	42657 MPa	43537 MPa
Thickness of carbon fiber sheet	0.55 mm/layer	

5.2.5 Production Process of Composite Specimen

The unidirectional carbon fiber sheet was cut into 40 mm-wide ×340 mm-long for impregnation with the epoxy resin. The bond area of 40×230 or 40×210 mm was selected to satisfy the effective bond length expression by Chen and Teng (2001) [45]. The fiber direction of the strip matched the longitudinal direction of 340 mm side of the concrete substrate.

To obtain good bond strength between FRP and concrete substrate, the concrete surface treatment is an important factor considered as the parameter of roughness in some specifications. In this study, the effect of different surface preparation was not the main focus, therefore, one of the standard methods, grinding, was used for the surface of the bond area on concrete substrate. Using a portable hand-angled grinder with a diamond grinding cup wheel shown in Figure 5.7, the substrate surface was grinded until the parts of coarse aggregate in concrete were exposed. For investigating two distinguished cases of surface condition, substrates of the 1st set were grinded to have much more coarse aggregate exposed on the substrate surface than those of the 2nd set. Figure 5.8 shows the difference of the substrate surface after the FRP debonding test. Figure 5.8(a) and (b) represent the concrete surface of the 1st set and the 2nd set, respectively. After grinding, the surface was cleaned to remove dust and small concrete particles with a water jet and dried until the bonding process at room temperature (Figure 5.9).

Figure 5.7 Angled Portable Grinder with Diamond Wheel Cup

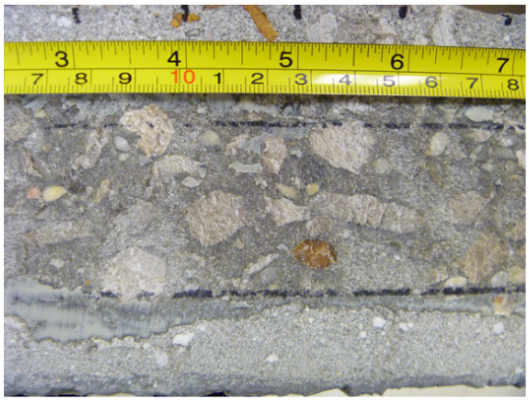

(a) 1st Set of Substrate Surface (More Exposed Aggregate

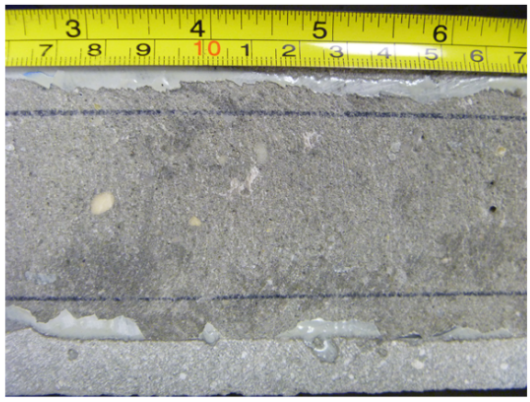

(b) 2st Set of Substrate Surface (Less Exposed Aggregate

Figure 5.8 Difference of Substrate Surface Preparation for 1st and 2nd Set

Figure 5.9 Grinded Bond Area of Concrete Substrate (1st Set)

Epoxy resin Sikadur 301 and Quakebond J300SR were prepared for priming the bond area of the substrate surfaces and impregnating the carbon fiber strips. Two components of Sikadur 301, A and B, were mixed prior the process as well as two components of Quakebond J300SR as shown in Figure 5.10. As a primer, the epoxy resin was applied in a thin and uniform layer to the bond area of concrete surface with a trim roller, and voids were stippled with a brush. The primer was cured at least 24 hours at room temperature and sanded lightly before FRP sheet application (Figure 5.11). In a flat square pan or on a flat surface of working table covered with a plastic sheet, the carbon fiber strips were fully impregnated with the epoxy resin (Sikadur 301 or Quakebond J300SR) and prepared in accordance with the manufacture's instruction. With a plastic spatula, a brush, or a roller, the epoxy resin was applied onto and was spread evenly until

the fabric was fully saturated as shown in Figure 5.12. The epoxy resin was also applied on the other side of the strips. After allowing the sheets to saturate thoroughly, excess resin was squeegeed off the sheets with a spatula before mounting the FRP sheets onto concrete substrate. Then, the FRP sheet was placed without wrinkles onto substrate and with a roller, pressed in longitudinal direction to remove trapped air. It is noted that the bond free zone by 50 mm from the edge of substrate was set by using masking tape on the concrete surface. After assembly, the specimens should not be moved or touched at least 45 minutes of workable time to harden. During this time, the sheet alignment or lifting can be corrected. The epoxy FRP bonded substrate was cured for 7 days at room temperature for the full bond strength before the pull-off test (Figure 5.13).

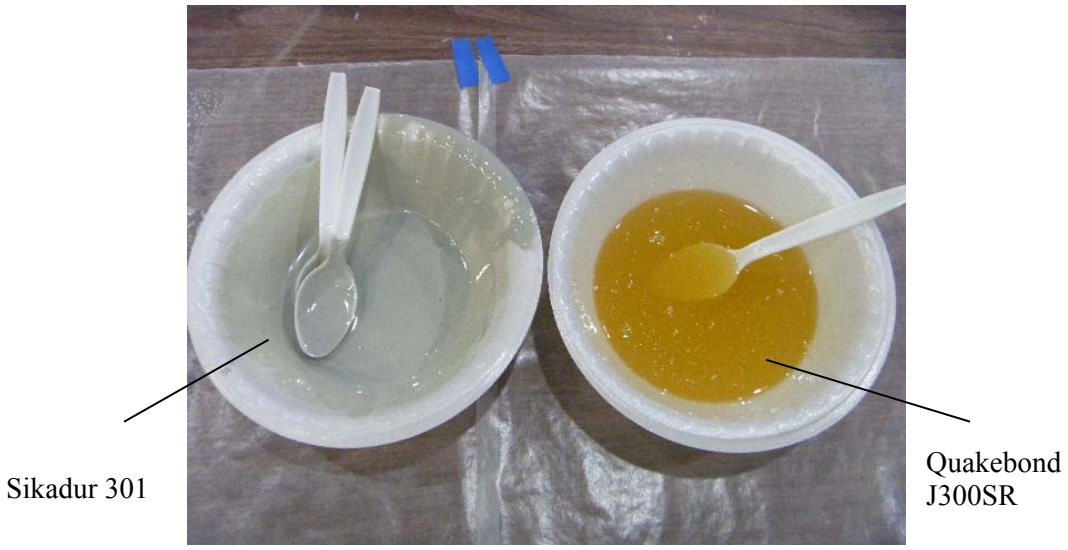

Figure 5.10 Mixed Epoxy Resin

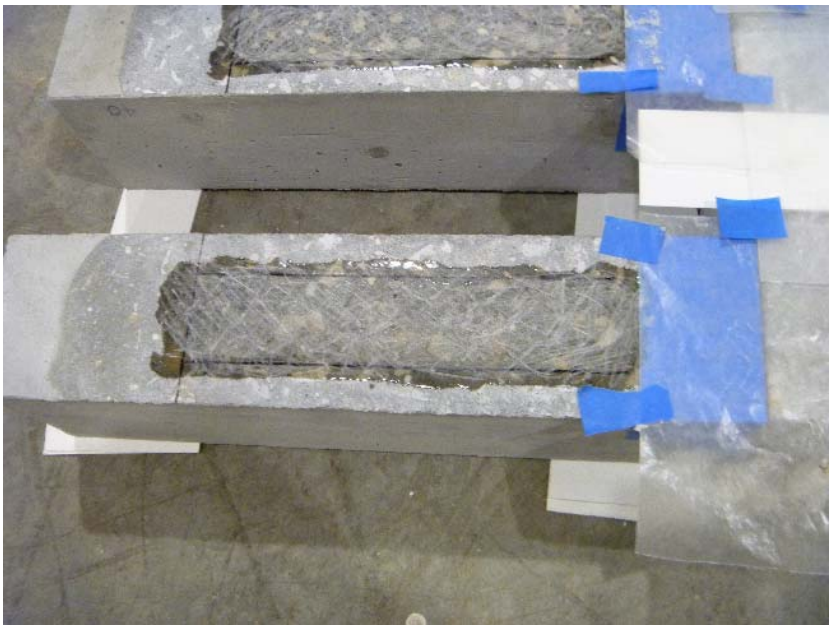

Figure 5.11 Primer on Bonded Area of Concrete Substrate

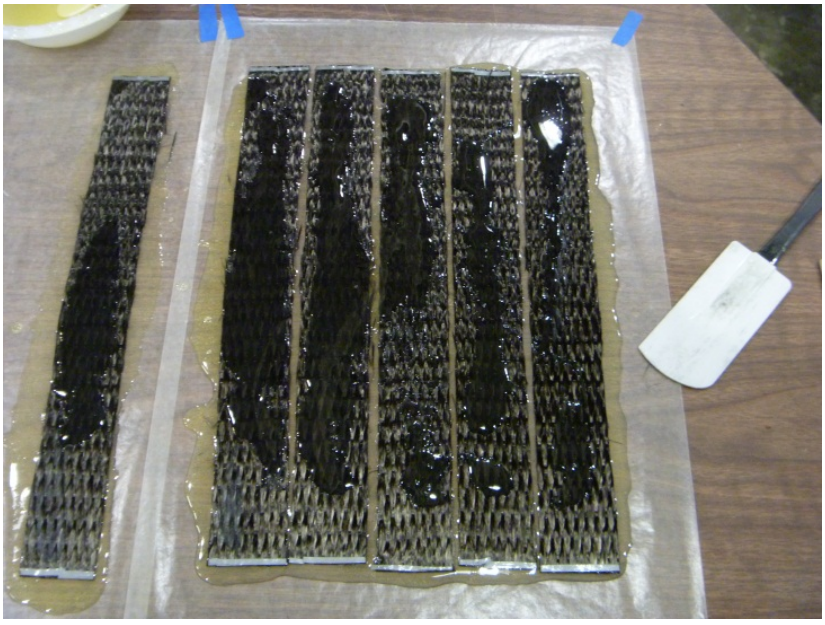

Figure 5.12 Impregnation Process of Carbon Fiber Strip with Epoxy Resin

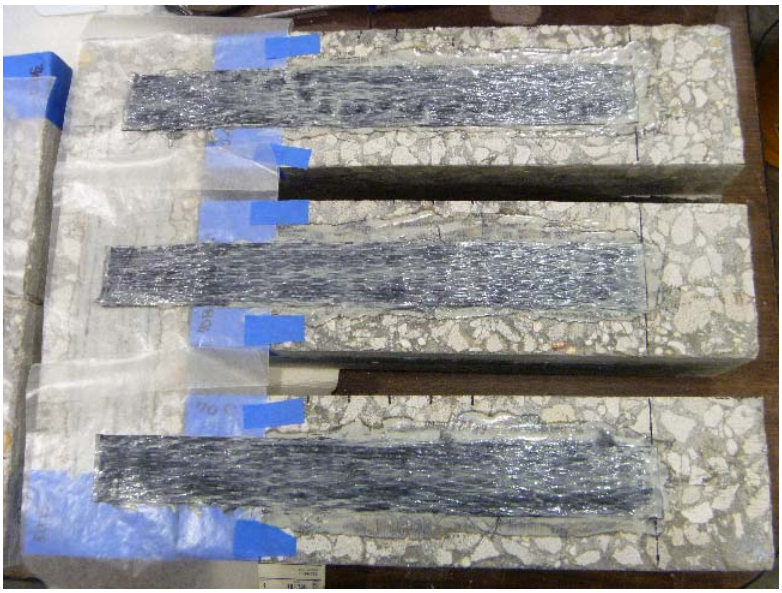

Figure 5.13 Curing Composite Material of FRP Strip Bonded to Substrate

5.3 FRP Pull-off Test

Using the MTS hydraulic powered tensile machine equipped with grip ends, a single pull-off test was performed on specimens. A metal frame was securely fixed to a metal plate, which was gripped at its bottom edge by the machine. On the plate and frame, composite concrete substrate was also fixed with one end of the FRP strip grabbed by the upper grip of the machine (Figure 5.14). The tensile machine with a load cell and the data acquisition system was connected to the computer to acquire and record the applied load level. The load was applied to the composite as the bottom actuator of the machine was moving downward in displacement controlled at the rate of 0.5mm/min until it resulted in failure as shown in Figure 5.15. All the data and the material properties used in the test are shown in Table 5.6.

Figure 5.14 Single Pull-off Test Setup

Figure 5.15 Debonded FRP Strip and Bond Area of Concrete Substrate

Table 5.6 Experimental Data with Maximum Transferable Loads

Specimen	Concrete compressive strength f_c' (MPa)	CFRP thickness t_p (mm)	Adhesive thickness t_a (mm)	Bond length L (mm)	Failure load P_{max} (kN)
20-A-sika	23.0	1.12	0.388	230	13.66
20-B-sika	23.0	1.12	0.350	230	16.90
20-C-sika	23.0	1.12	0.228	230	14.62
30-A-sika	30.8	1.12	0.422	230	14.64
30-B-sika	30.8	1.12	0.273	230	9.86
30-C-sika	30.8	1.12	0.485	230	15.88
70-A-sika	74.5	1.12	0.510	230	16.33
70-B-sika	74.5	1.12	0.202	230	18.09
70-C-sika	74.5	1.12	0.418	230	18.29
20-1-sika	23.0	1.12	0.547	200	13.16
20-2-sika	23.0	1.12	0.352	200	13.64
20-3-sika	23.0	1.12	0.305	200	12.86
30-1-sika	30.8	1.12	0.457	200	16.29
30-2-sika	30.8	1.12	0.647	200	16.94
30-3-sika	30.8	1.12	0.285	200	16.57
70-1-sika	74.5	1.12	0.693	200	15.22
70-2-sika	74.5	1.12	0.363	200	15.99
70-3-sika	74.5	1.12	0.528	200	15.88
25-1-sika	28.2	1.55	0.353	200	10.95
25-2-sika	28.2	1.65	0.403	200	11.92
25-3-sika	28.2	1.5	0.450	200	11.01
25-1-QW	28.2	1.7	0.215	200	12.79
25-2-QW	28.2	1.65	0.244	200	11.84
25-3-QW	28.2	1.65	0.187	200	11.05
40-1-sika	39.1	1.45	0.290	200	11.38
40-2-sika	39.1	1.4	0.186	200	11.14
40-3-sika	39.1	1.5	0.272	200	11.64
40-1-QW	39.1	1.7	0.220	200	12.90
40-2-QW	39.1	1.65	0.278	200	13.55
40-3-QW	39.1	1.7	0.162	200	13.53
25-a-sika	28.2	1.03	0.460	200	9.52
25-b-sika	28.2	1.12	0.120	200	11.17
25-c-sika	28.2	1.12	0.070	200	12.45
25-a-QW	28.2	1.8	0.420	200	13.50
25-b-QW	28.2	1.5	0.193	200	12.16
25-c-QW	28.2	1.65	0.446	200	12.82
40-a-sika	39.1	1.12	0.292	200	11.68
40-b-sika	39.1	1.12	0.208	200	11.47
40-c-sika	39.1	1.12	0.260	200	11.03
40-a-QW	39.1	1.7	0.438	200	13.05
40-b-QW	39.1	1.65	0.242	200	14.04
40-c-QW	39.1	1.7	0.365	200	15.03

b_p = 40 mm; Concrete substrate size is 100×80×350 mm; E_p = 42657 MPa and 43537 MPa for specimen sika and QW, respectively; E_a = 2000 MPa and 1995 MPa for specimen sika and QW, respectively; v_a = 0.4 for both adhesives; G_a = $E_a/2(1 + v_a)$.

CHAPTER V

ANALYSIS AND COMPARISON

6.1 Parameter Analysis

To apply the proposed criterion and the developed analytical solution, the fracture depth and strength factor was determined in this section. The fracture depth was determined from experimental measurements, and the strength factor was assessed performing regression analysis on the experimental results.

The fracture depth is the parameter with physical meaning in the bond strength expression derived in Chapter III. As a similar concept, several studies tried to correlate the bond strength to the microscopic configuration of the FRP bond system ([67]□[70]). For quantifying the fracture depth which is the crack initiation point at a certain depth in concrete substrate, the experimental work shown in Chapter V was utilized. The thickness of the concrete layer attached to the debonded FRP strips was obtained at ten points along the bond length for each specimen. It was observed that the amount of concrete attached to the FRP strips peeled less concrete off substrate for relatively high compressive strength. From this inference, the fracture depth was related to concrete compressive strength. The relation between the fracture depth and concrete compressive

strength was examined by plotting the measurement results. Figure 6.1 shows a trend line for the fracture depth expressed as

$$t = \frac{4.5}{\sqrt{f_c'}}. \tag{6.1}$$

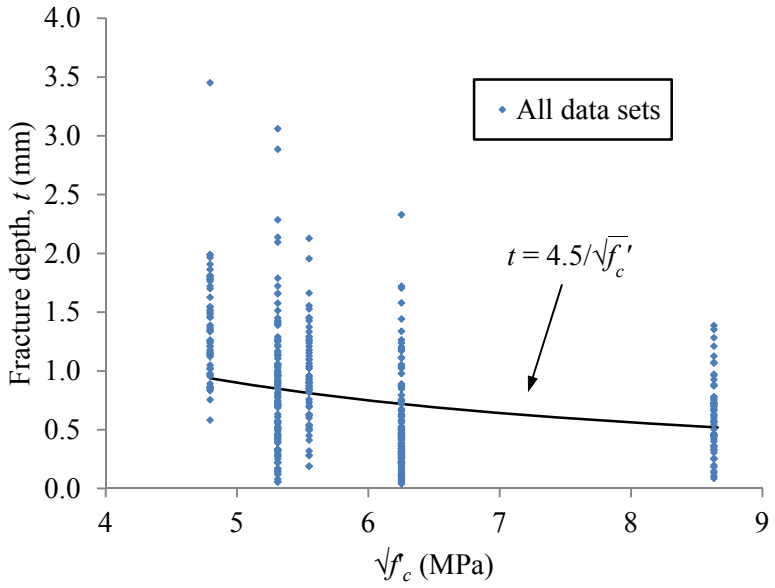

Figure 6.1 Plot of Fracture Depth vs. Square Root of Concrete Compressive Strength

The strength factor is a coefficient applied for concrete tensile strength to yield the limit bond stress between FRP and concrete, which is the tensile strength of a concrete finite element just below the bond interface. For determining the strength factor, regression analysis was carried out on the experimental results by applying the obtained

fracture depth (Equation (6.1)). Similar to the fracture depth, the strength factor was also related to concrete compressive strength. With a MATLAB program, adequate strength factors for each specimen were obtained for the first and the second data set. These values were plotted to obtain the strength factor as a function of the square root of concrete compressive strength. The result from regression analysis is shown in Figure 6.2. From analysis, strength factors for each data set are expressed as follows;

$$\alpha_1 = \frac{765}{\sqrt{f'_c}} \tag{6.2}$$

$$\alpha_2 = \frac{330}{\sqrt{f'_c}} \tag{6.3}$$

where α_1 and α_2 are strength factors for the first and the second data set, respectively. The strength factor for the first data set achieved relatively higher values as compared to the second data set. Considering determined expressions for strength factors, the potential bond strength, which is concrete tensile strength, tends to be maximized in the first data set. In contrast, the strength factor for the second data set actually reduces the possible maximum bond strength. This analysis indicated that the bond strength between FRP and concrete with much coarse aggregate exposed on the surface was more resilient against shear and/or tensile stress than that of FRP and concrete exposing less coarse aggregate. Obtaining two distinguishable expressions, the strength factor for the average surface condition would be determined and applied for predicting the bond strength. The trend line for the strength factor for general application is shown in Figure 6.2 as a function of the square root of concrete compressive strength and expressed as

$$\alpha_{avg} = \frac{485}{\sqrt{f'_c}}. \tag{6.4}$$

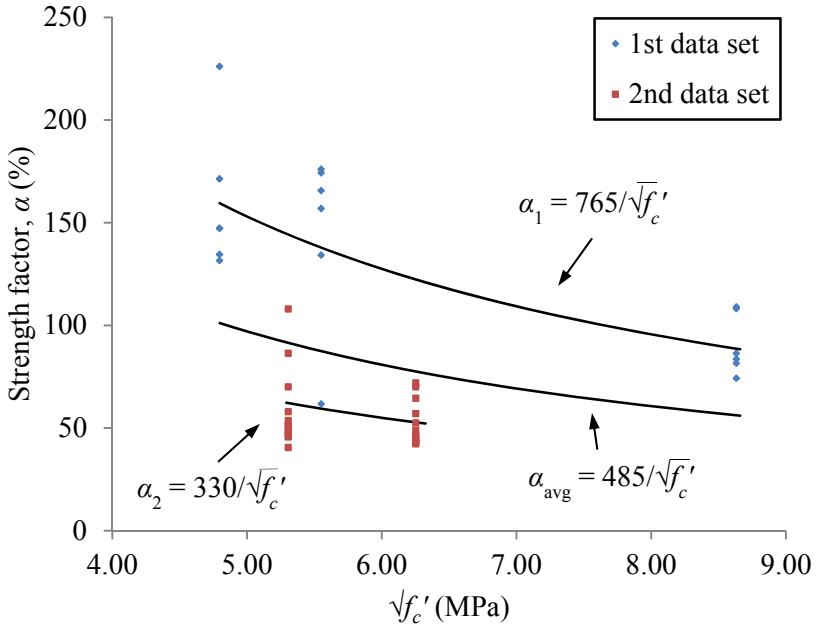

Figure 6.2 Plot of Strength Factor vs. Square Root of Concrete Compressive Strength

6.2 Comparison with Experimental Values

For comparison, the existing experimental data from different studies (Chajes et al. (1996) [71], Maeda et al. (1997) [28], Täljsten (1997) [72], Ueda et al. (1999) [73], Zhao et al. (2000) [74], Adhikary (2001) [75], Xu et al. (2001) [76], Nakaba et al. (2001) [31], Wu et al. (2001) [77], Tan (2002) [78], Ren (2003) [79], Dai et al. (2005) [51], Yao et al. (2005) [58], Sharma et al. (2006) [80], and Toutanji et al. (2007) [81]) and those

conducted in this study were used (totally 342 data points). In the collected data, FRP specimens consisted of carbon fiber or glass fiber and various types of adhesive materials. In most cases, adhesive material properties were ignored and not provided in literature. For these cases, the adhesive thickness, Young's modulus, and Poisson's ratio were reasonably assumed as t_a = 1 mm, E_a = 1995 MPa (Quakebond J300SR), and v_a = 0.4. The comparisons of the prediction with experimental results were performed using each strength factor α_1, α_2, and α_{avg} to understand the effect of different strength factors. The predicted values and experimental values were plotted and analyzed with statistical indicators. The average ratio of the experimental value to the predicted value and the correlation factor were obtained for each comparison. The plots of the comparison results are shown in Figure 6.3 to 6.5. With the strength factor α_1, the average ratio of 0.726 indicated that the prediction value tends to be higher than the corresponding experimental value (Figure 6.3). Applying the strength factor α_2, the prediction became relatively low compared to the experimental results with the average ratio of 1.402 (Figure 6.4). The prediction with the strength factor α_{avg} seemed more suitable (Figure 6.5). By recognizing the substrate surface condition, it is possible to choose either strength factor α_1 or α_2 for each specimen to predict more reasonable bond strength. In such an ideal case, the predictions are shown in Figure 6.6. The only limitation in the application of the proposed criterion and expression is the adhesive property data.

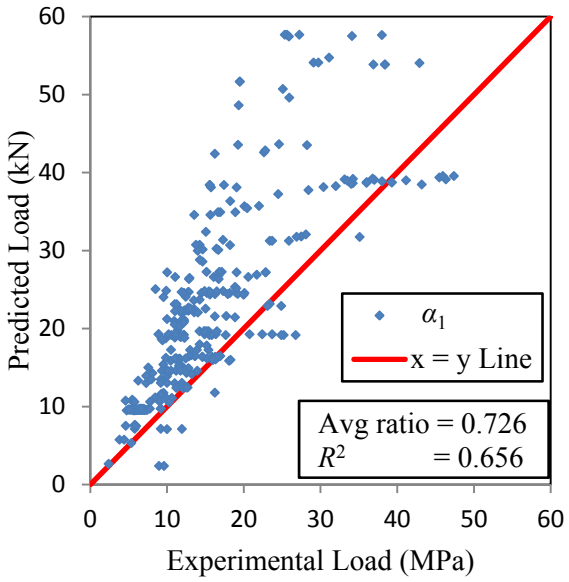

Figure 6.3 Predicted P_{max} by Proposed Expression with α_1 vs. Experimental P_{max}

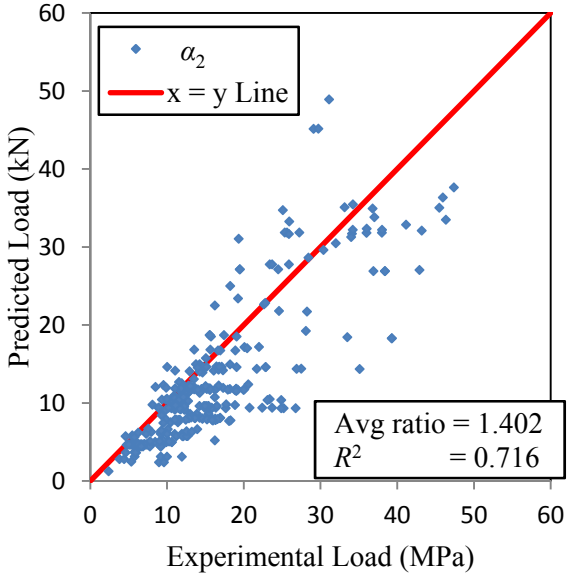

Figure 6.4 Predicted P_{max} by Proposed Expression with α_2 vs. Experimental P_{max}

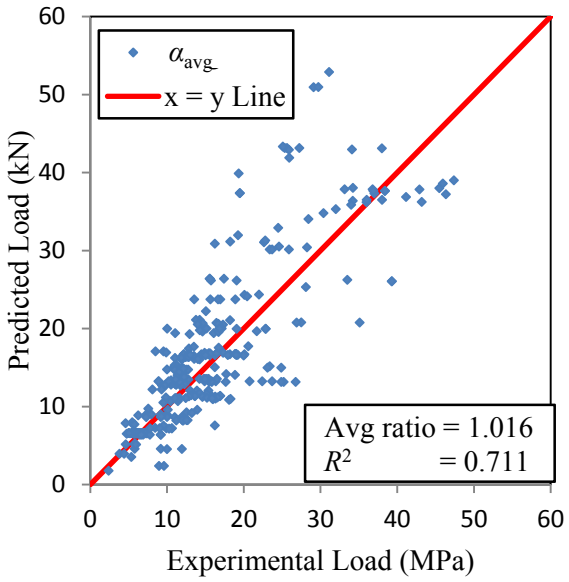

Figure 6.5 Predicted P_{max} by Proposed Expression with α_{avg} vs. Experimental P_{max}

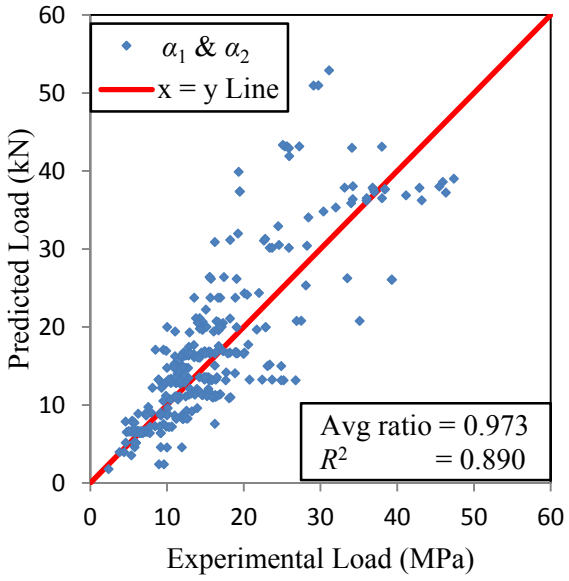

Figure 6.6 Predicted P_{max} by Proposed Expression with α_1 & α_2 vs. Experimental P_{max}

6.3 Comparison with Existing Models

In order to verify the applicability of the proposed criterion, the proposed model was compared with conventional models. The bond strength for collected 300 data points from literature and those collected in this study (42 points) were predicted by using six existing prediction models (Neubauer & Rostásy (1997) [37], Brosens (2001) [52], Chen & Teng (2001) [45], Dai et al. (2005) [51], Lu et al. (2005) [50], and Karbhari et al. (2006) [54]). From the prediction and the experimental value, statistical indicators were obtained for each model. The results of the comparison are shown in Table 6.1. Also, plots of the predicted maximum transferable load versus the experimental value are shown in Figure 6.7 to 6.12.

Table 6.1 Comparison between Existing Models and Proposed Expression

Prediction Models for P_{max}	Average ratio of P_{max}(Experiment)/ P_{max}(Prediction)	Correlative factor R^2
Neubauer & Rostásy (1997) [37]	0.980	0.790
Brosens (2001) [52]	0.568	0.797
Chen & Teng (2001) [45]	1.163	0.826
Dai et al. (2005) [51]	1.599	0.416
Lu et al. (2005) [50]	1.152	0.836
Karbhari et al. (2006) [54]	0.778	0.753
Proposed expression with α_1	0.726	0.656
Proposed expression with α_2	1.402	0.716
Proposed expression with α_{avg}	1.016	0.711

Prediction values were obtained for the collected 342 data points.

The proposed expression with the strength factor α_{avg} showed good agreement with the experimental results in terms of the average ratio of 1.016. Among the six existing models, this average ratio was the most reasonable value. Neubauer & Rostásy's model (1997) [37] also showed the reliable average ratio of 0.980 with the empirical expression for the interfacial fracture energy as $G_f = 0.202 f_t$. Models by Chen & Teng (2001) [45] and Lu et al. (2005) [50] provided a relatively good average ratio although they underestimated the bond strength. In terms of the correlation factor R^2, the predictions by these two models were in consistency with R^2 of 0.836 and 0.826, respectively. The proposed expression with α_{avg} showed a relatively good consistency with the correlation factor of 0.711. In six existing models, Karbhari et al.'s (2006) [54] was the only model considering the adhesive properties as parameters in the expression for G_f except for the proposed expression. However, the prediction result provided a relatively low correlative factor of 0.416 with the average ratio of 1.599. Compared with other models, the proposed expression could predict the bond strength with various material properties and geometric configurations based on the criterion for the debonding initiation mechanism.

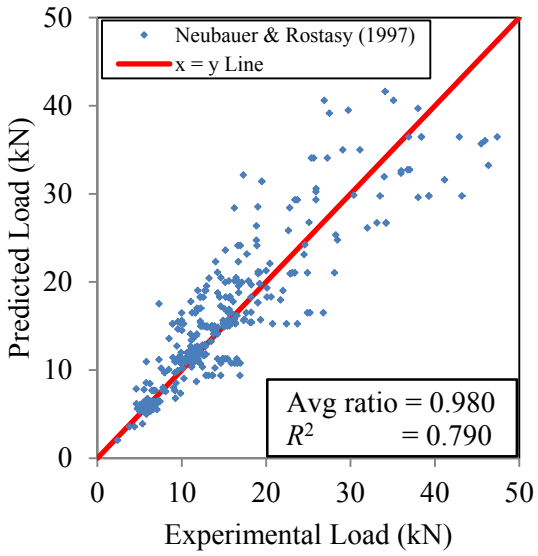

Figure 6.7 Neubauer & Rostásy's Model (1997) [37] vs. Experimental P_{max}

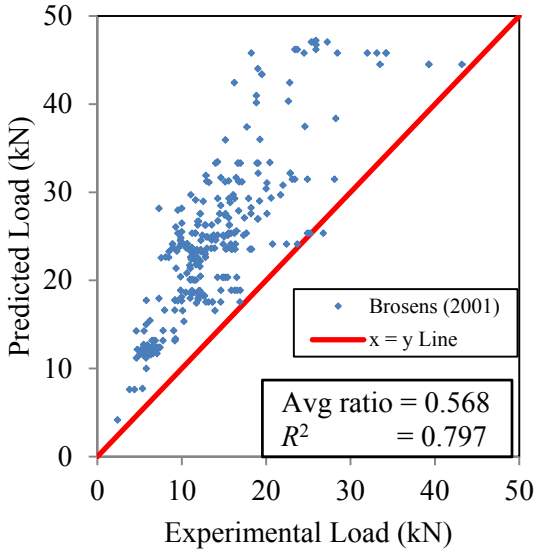

Figure 6.8 Brosens' Model (2001) [52] vs. Experimental P_{max}

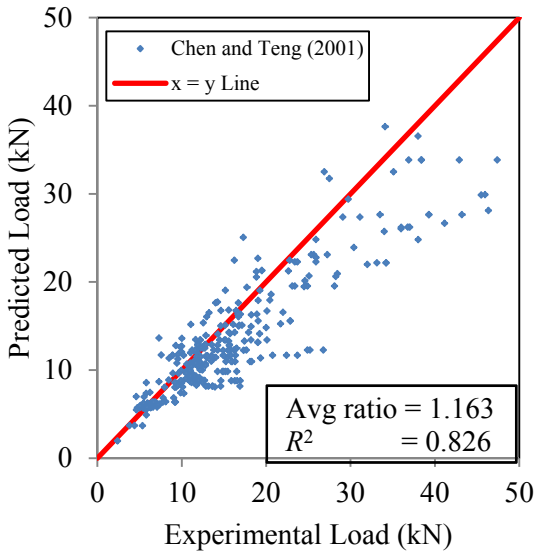

Figure 6.9 Chen & Teng's Model (2001) [45] vs. Experimental P_{max}

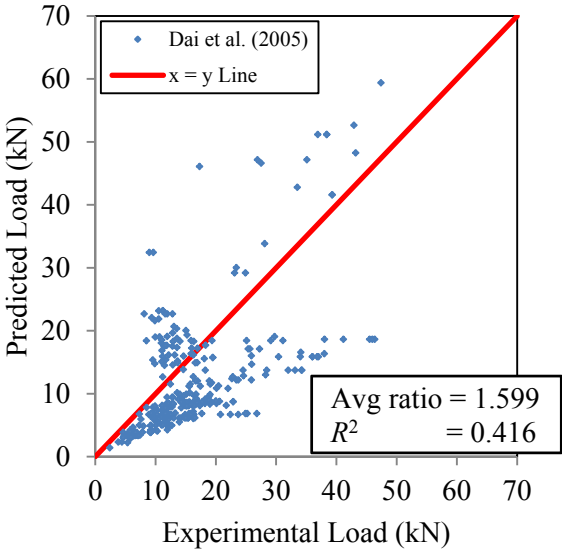

Figure 6.10 Dai et al.'s Model (2005) [51] vs. Experimental P_{max}

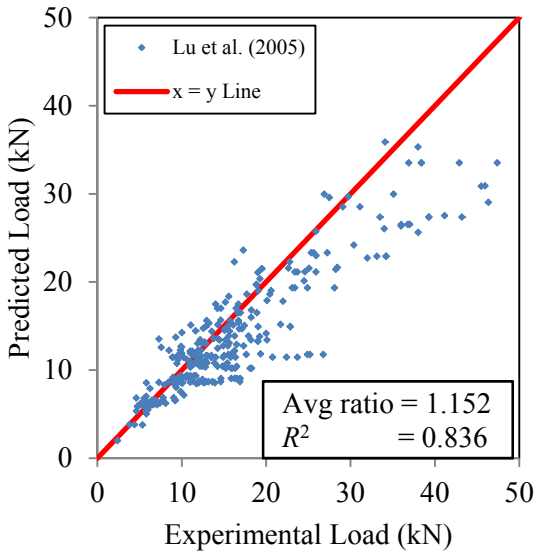

Figure 6.11 Lu et al.'s Model (2005) [50] vs. Experimental P_{max}

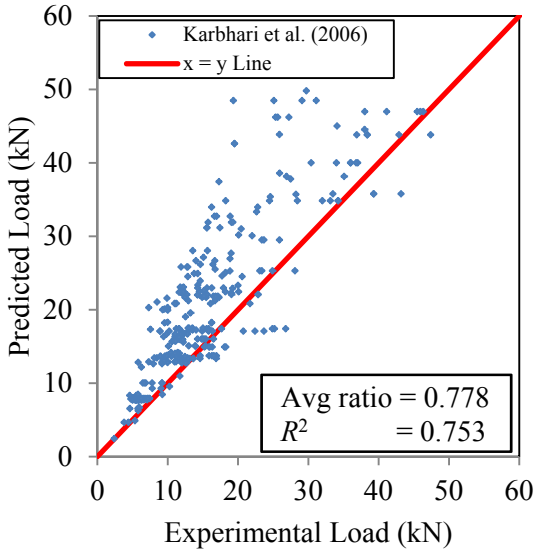

Figure 6.12 Karbhari et al.'s Model (2006) [54] vs. Experimental P_{max}

CHAPTER VI

CONCLUSIONS

A criterion on debonding initiation was proposed to determine the critical stress state in substrate by implementing concrete tensile strength. Introducing the strength factor, concrete tensile strength was modified to be considered as the limit bond stress for the FRP to concrete bond interface. The strength factor was determined capturing the effect of the substrate surface condition. For applying the proposed criterion, the stress state on a finite element in concrete substrate was expressed by using the elasticity theory. The expression for the stress state was given as a function of the interfacial shear distribution and the fracture depth presenting the microscopic failure depth. The fracture was defined that the concrete failure initiates due to the local critical stress state. The strength factor and the fracture depth were determined as a function of the square root of concrete compressive strength from an in-house experimental result.

An analytical solution was developed for the FRP local slip based on mechanics of materials. By this solution, the constitutive slip-shear behavior of the bond interface was captured corresponding to a certain loading level on the FRP strip. The expressions for the interfacial shear stress distribution and the corresponding local slip were also

determined. In these expressions, adhesive material properties such as thickness, Young's modulus, and Poisson's ratio were considered as parameters, which are often neglected. The values for the maximum interfacial shear stress and the corresponding local slip were obtained by applying the proposed criterion and the analytical solution. The interfacial fracture energy expressed as a function of these two values was successfully obtained for each bond system.

The predicted values for the collected 342 data points showed good agreement with experimental results for verification of the proposed criterion and expression. Also, the comparison with other existing models verified the applicability of the proposed criterion and expression providing a reasonably high correlation factor.

APPENDIX

The detailed derivation process for the developed analytical solution is shown here.

Take a small segment of the bond interface of FRP to concrete substrate in Figure A.1.

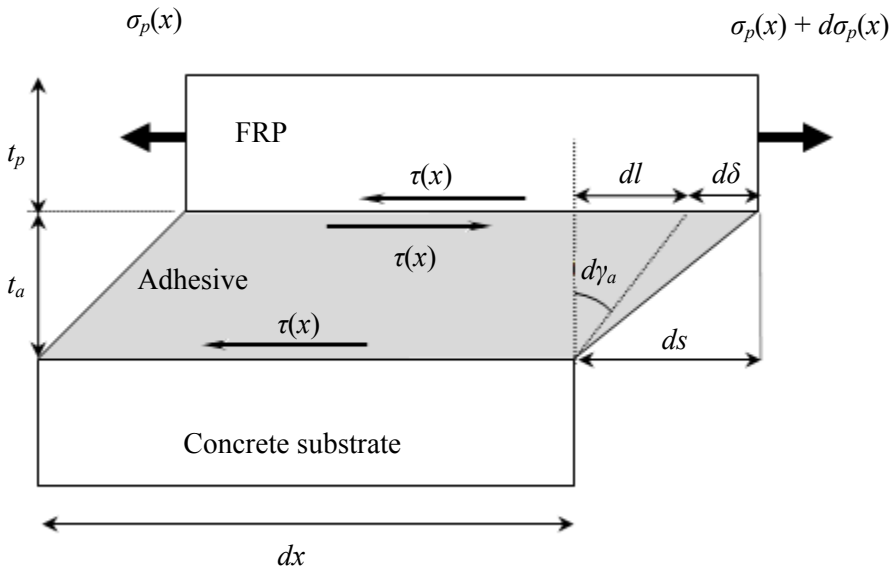

Figure A.1 Small Segment of Bond Interface of FRP to Concrete Substrate

Force equilibrium in the axial direction can be as

$$\tau(x) b_p dx = d\sigma_p b_p t_p \tag{A.1}$$

and b_p in both sides are canceled each other to yield

$$\tau(x) dx = d\sigma_p t_p \tag{A.2}$$

or

$$\tau(x) = \frac{d\sigma_p}{dx} t_p . \tag{A.3}$$

Governing equation on the FRP local slip, denoted as s, is expressed as the sum of the shear deformation and the axial elongation as

$$s = l + \delta \tag{A.4}$$

where l = the shear deformation and δ = the axial elongation of adhesive. Take the differential of Equation (A.4) gives

$$\frac{ds}{dx} = \frac{dl}{dx} + \frac{d\delta}{dx} . \tag{A.5}$$

Fundamental mechanics of materials based on the elasticity theory shows the stress-strain relations for those deformations above as followings:

The stress-strain on FRP

$$\frac{ds}{dx} = \frac{\sigma_p(x)}{E_p} \tag{A.6}$$

The stress-strain on adhesive at the interface to FRP

$$\frac{d\delta}{dx} = \frac{\sigma_a(x)}{E_a} \tag{A.7}$$

The shear deformation on adhesive

$$\tau(x) = G_a \gamma_a = G_a \frac{l(x)}{t_a} \tag{A.8}$$

Consider two consecutive small segments of the adhesive layer on the bond interface to FRP as shown in Figure A.2.

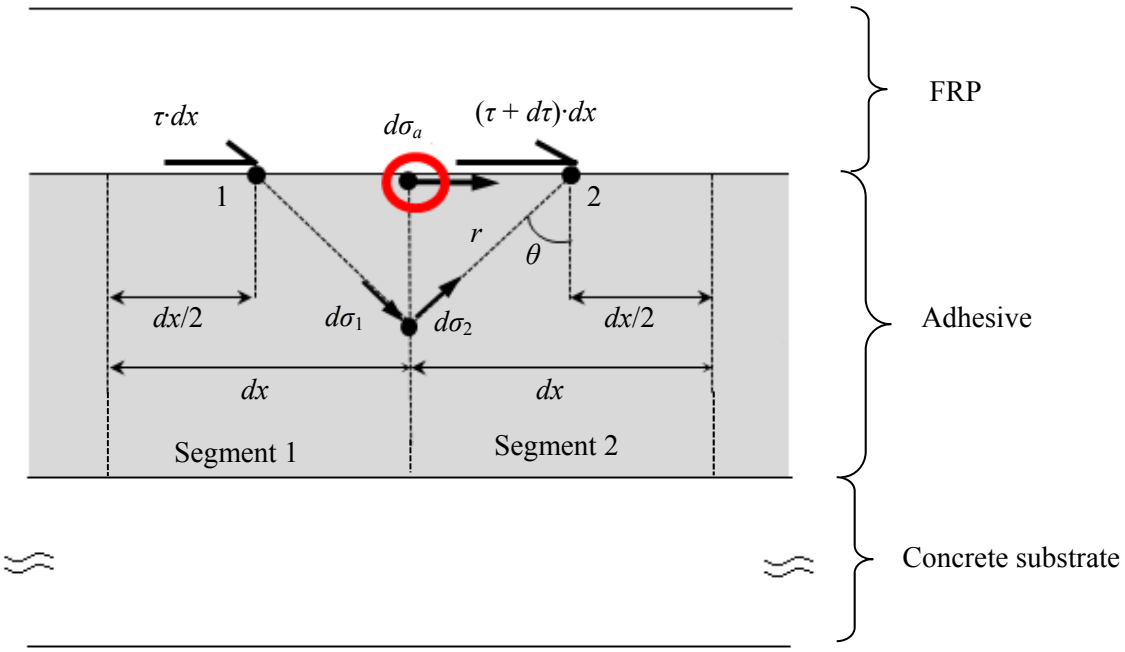

Figure A.2 Small Segment of Adhesive Layer at Interface to FRP

The stress state at any point on the interface of the two segments induced by the differential load τdx at the point 1 is expressed as

$$d\sigma_1 = \frac{2(\tau \cdot dx)}{\pi r}\sin\theta \tag{A.9}$$

where r = the radial distance from the loading point to the considered element and θ = the angle between the vertical line at the loading point toward the inside of material and the radial line from the loading point to the considered element with clockwise positive.

Also, on the same element with the stress state $d\sigma_1$, the stress state induced by the load $(\tau + d\tau)\,dx$ at the point 2 is expressed as

$$d\sigma_2 = \frac{2\{(\tau + d\tau)dx\}}{\pi r}\sin\theta \tag{A.10}$$

Adding those stress states at the interface to FRP, which is the upper edge of the adhesive layer, the axial stress state $d\sigma_a$ is determined with $r = dx/2$ and $\theta = \pi/2$ for the load τdx and $\theta = \pi/2$ for the load $(\tau + d\tau)\,dx$ as following;

$$\begin{aligned} d\sigma_a &= d\sigma_1 + d\sigma_2 \\ &= \frac{2(\tau \cdot dx)}{\pi\frac{dx}{2}}\sin\left(\frac{-\pi}{2}\right) + \frac{2\{(\tau + d\tau)dx\}}{\pi\frac{dx}{2}}\sin\left(\frac{\pi}{2}\right) \end{aligned} \tag{A.11}$$

and it is simplified to have the expression for $d\sigma_a$ as

$$d\sigma_a = \frac{4d\tau}{\pi}. \tag{A.12}$$

Substituting Equation (A.6)□(A.8) into Equation (A.5) to yield

$$\frac{\sigma_p(x)}{E_p} = \frac{d}{dx}\left\{\frac{t_a}{G_a}\tau(x)\right\} + \frac{\sigma_a(x)}{E_a}. \tag{A.13}$$

Take the derivative of Equation (A.13) to have the following;

$$\frac{1}{E_p}\frac{d\sigma_p}{dx} = \frac{t_a}{G_a}\frac{d^2\tau}{dx^2} + \frac{1}{E_a}\frac{d\sigma_a}{dx}. \tag{A.14}$$

Substituting Equation (A.3) and (A.12) into Equation (A.14) gives

$$\frac{1}{E_p}\frac{\tau}{t_p} = \frac{t_a}{G_a}\frac{d^2\tau}{dx^2} + \frac{1}{E_a}\frac{4}{\pi}\frac{d\tau}{dx} \tag{A.15}$$

or

$$\frac{d^2\tau}{dx^2} + \frac{G_a}{t_a}\frac{1}{E_a}\frac{4}{\pi}\frac{d\tau}{dx} - \frac{G_a}{t_a}\frac{1}{E_p t_p}\tau = 0\,. \tag{A.16}$$

From Equation (A.16), the 2nd order differential equation in terms of τ is developed as;

$$\tau'' + A\tau' - B\tau = 0 \tag{A.17}$$

$$A = \frac{4G_a}{\pi E_a t_a} \tag{A.18}$$

$$B = \frac{G_a}{E_p t_p t_a}\,. \tag{A.19}$$

For solving Equation (A.17) for τ, the characteristic equation turns out to be

$$\lambda^2 + A\lambda - B = 0 \tag{A.20}$$

where λ = the roots for a solution. Solving Equation (A.20) for λ yields the positive root λ_1 and the negative root λ_2.

A solution for Equation (A.17) is expressed as

$$\tau(x) = C_1 e^{\lambda_1 x} + C_2 e^{\lambda_2 x} \tag{A.21}$$

where C_1 and C_2 are constants determined with boundary conditions (B.C.).

B.C. at the free end, x = 0, is no interfacial shear stress based on experiments, and the expression is $\tau(0) = 0$. This condition yields $C_1 = -C_2$, and Equation (A.21) becomes

$$\tau(x) = C_1\left(e^{\lambda_1 x} - e^{\lambda_2 x}\right) \tag{A.22}$$

Substituting Equation (A.22) into Equation (A.3) gives

$$\frac{d\sigma_p}{dx} = \frac{C_1}{t_p}\left(e^{\lambda_1 x} - e^{\lambda_2 x}\right). \tag{A.23}$$

Take the integral of Equation (A.23) from 0 to x, and the expression for $\sigma_p(x)$ is given as

$$\sigma_p(x) = \frac{C_1}{t_p}\left(\frac{e^{\lambda_1 x}-1}{\lambda_1} - \frac{e^{\lambda_2 x}-1}{\lambda_2}\right). \tag{A.24}$$

Another B.C. on the stress in FRP at the loaded end $x = L$ is expressed as $\sigma_p(L) = P_{app}/b_p t_p$ where P_{app} is the applied tensile load level at the end of the FRP strip. From Equation (A.24), the coefficient C_1 is expressed as

$$\frac{C_1}{t_p}\left(\frac{e^{\lambda_1 L}-1}{\lambda_1} - \frac{e^{\lambda_2 L}-1}{\lambda_2}\right) = \frac{P_{app}}{b_p t_p} \tag{A.25}$$

or

$$C_1 = \frac{P_{app}}{b_p} K \tag{A.26}$$

where

$$K = \left(\frac{e^{\lambda_1 L}-1}{\lambda_1} - \frac{e^{\lambda_2 L}-1}{\lambda_2}\right)^{-1}. \tag{A.27}$$

Then, using K (Equation (A.27)), the expression for $\tau(x)$ is expressed as

$$\tau(x) = \frac{P_{app}}{b_p} K\left(e^{\lambda_1 x} - e^{\lambda_2 x}\right). \tag{A.28}$$

Determining the expression for $s(x)$, use Equation (A.5) with the substitution of Equation (A.7) and (A.8) to yield

$$\frac{ds}{dx} = \frac{t_a}{G_a}\tau' + \frac{\sigma_a}{E_a}. \tag{A.29}$$

Substituting Equation (A.12) into Equation (A.29) and taking the integral of it from 0 to x, the expression for $s(x)$ is obtained as

$$s(x) = \frac{P_{\text{app}}}{b_p} K \left\{ \frac{t_a}{G_a} \left(e^{\lambda_1 x} - e^{\lambda_2 x} \right) + \frac{4}{\pi E_a} \left(\frac{e^{\lambda_1 x} - 1}{\lambda_1} - \frac{e^{\lambda_2 x} - 1}{\lambda_2} \right) \right\}. \tag{A.30}$$

To find the expression for $\tau(x)$ at the certain load level such that the interfacial maximum shear stress $\tau_{\max}$ occurs, use the notation for such applied load as $P_{\text{app\_}\tau\max}$. Assuming $\tau_{\max}$ reaches at the loaded end ($x = L$) for the debonding initiation, the condition is expressed as $\tau(L) = \tau_{\max}$. Then, the expression for $\tau_{\max}$ is determined in terms of $P_{\text{app\_}\tau\max}$ as

$$\tau_{\max} = \frac{P_{\text{app\_}\tau\max}}{b_p} K \left(e^{\lambda_1 L} - e^{\lambda_2 L} \right). \tag{A.31}$$

From Equation (A.31), the expression for $P_{\text{app\_}\tau\max}$ is solved as

$$P_{\text{app\_}\tau\max} = \tau_{\max} \frac{b_p}{K \left(e^{\lambda_1 L} - e^{\lambda_2 L} \right)}. \tag{A.32}$$

Substitute Equation (A.32) back into Equation (A.28), the expression for $\tau(x)$ when $\tau_{\max}$ occurs is determined as

$$\tau(x) = \tau_{\max} \frac{e^{\lambda_1 x} - e^{\lambda_2 x}}{e^{\lambda_1 L} - e^{\lambda_2 L}}. \tag{A.33}$$

Also, the expression for the local slip corresponding to the maximum interfacial shear stress, denoted as s_0, is determined at $x = L$ by substituting Equation (A.32) into Equation (A.30) as the following;

$$s_0 = s(L) = \frac{\tau_{\max}}{e^{\lambda_1 L} - e^{\lambda_2 L}} \left\{ \frac{t_a}{G_a} \left(e^{\lambda_1 L} - e^{\lambda_2 L} \right) + \frac{4}{\pi E_a} \left(\frac{e^{\lambda_1 L} - 1}{\lambda_1} - \frac{e^{\lambda_2 L} - 1}{\lambda_2} \right) \right\}. \tag{A.34}$$

Equation (A.33) and (A.34) are simplified by considering $\exp(\lambda_1 L) >> \exp(\lambda_2 L)$ for most cases, and expressions are given by

$$\tau(x) = \tau_{\max} \frac{e^{\lambda_1 x} - e^{\lambda_2 x}}{e^{\lambda_1 L}} \tag{A.35}$$

$$s_0 = \tau_{\max}\left(\frac{t_a}{G_a} + \frac{4}{\lambda_1 \pi E_a}\right). \tag{A.36}$$

REFERENCES

[1] Kaw, A. K., *Mechanics of Composite Materials Second Edition*, Taylor & Francis Group, LLC, New York, 2006.

[2] Meier, U., Deuring, M., Meier, H., and Schwegler, G., CFRP bonded sheets. *In: Fiber-Reinforced-Plastic (FRP) reinforcement for concrete structures: Properties and applications*, Elsevier Science Publishers B. V., Netherlands, 1993.

[3] Bank, L. C., *Composites for Construction: Structural Design with FRP Materials*, John Wiley & Sons, Inc., Hoboken, New Jersey, 2006.

[4] Seible, F. and Karbhari, V., *Advanced Composites for Civil Engineering Applications in the United States*, Proceedings of the 1st International Conference on Composites in Infrastructure, National Science Foundation, Tucson, Arizona, 1996.

[5] Takeo, A., *Development of Carbon Fiber Industry Past and Future*, Proceedings of 9th US/Japan Conference on Composites Materials, Japan, 2000.

[6] Fleming, C. J. and King, G. E. M., *The developments of structural adhesives for three original uses in South Africa*, Proceedings of RILEM Symposium on Synthetic Resins in Building Construction, Paris, pp. 75−92, 1967.

[7] Van Gemert, D., *Repairing of concrete structures by externally bonding steel plates*, Proceedings of ICP/RILEM/IBK International Symposium on Plastics in Material, Prague, pp. 519□526, 1981.

[8] Iino, T. and Otokawa, K., *Application of Epoxy Resins in Strengthening of Concrete Structures*, Proceedings of 3rd International Congress on Polymers in Concrete, Koriyama, Japan, Vol. 2, pp. 997□1011, 1981.

[9] Ladner, M. and Weder, C., *Concrete Structures with Bonded External Reinforcement*, EMPA Report No. 206, Dubendorf, Switzerland (in German).

[10] Macdonald, M. D., *The Flexural Performance of 3.5m Concrete Beams with Various Bonded External Reinforcements*, Department of the Environment, TRRL Report SR 728, Crowthorne, 1982.

[11] Swamy, R. N., Jones, R., and Bloxham, L. W., *Structural Behavior of Reinforced Concrete Beams Strengthened by Epoxy-Bonded Steel Plates*, The Structural Engineer, Vol. 65, No. 2, pp. 59−68, 1987.

[12] Quantrill, R. J. and Hollaway, L. C., *The Flexural Rehabilitation of Reinforced Concrete Beams by the Use of Prestressed Advanced Composite Plates*, Composites Science and Technology, Vol. 58, No. 8, pp. 1259□1275, 1998.

[13] Saadatmanesh, H. and Ehsani, M. R., *RC Beams Strengthened with GFRP Plates. I: Experimental Study*, Journal of Structural Engineering, Vol. 117, No. 11, pp. 3417□3433, 1991.

[14] Wei, A., Saadatmanesh, H., and Ehsani, M. R., *RC Beams Strengthened with FRP Plates II: Analysis and Parametric Sstudy*, Journal of Structural Engineering, Vol. 117, No. 11, pp. 3434□3455, 1991.

[15] Triantafillou, T. C. and Plevris, N., *Strengthening of RC Beams with Epoxy-Bonded Fibre-Composite Materials*, Materials and Structures, Vol. 25, No. 4, pp. 201□211, 1992.

[16] Ritchie, P. A., Thomas, D. A., Lu, L. W., and Connelly, G. M., *External Reinforcement of Concrete Beams Using Fiber Reinforced Plastics*, ACI Structural Journal, Vol. 88, No.4, pp. 490□500, 1991.

[17] Rostasy, F. S., *Strengthening of R/C- and P/C-structures with Bonded Steel and FRP Plates*, Proceedings of the 5th International Conference on Structural Faults and Repair, University of Edinburgh, Vol.2, pp. 217□224, 1993.

[18] Shijie, W. and Ruixian, Z., *The Study of Fiber Composite Plates for Strengthening Reinforced Bridges*, Proceedings of ICCM-9, Madrid, Vol.6, pp. 224□231, 1993.

[19] Parmeswaran, V. S., Neelamegam, M., and Dattatreya, J. K., *Use of Non-Ferrous Externally Bonded Reinforcement for Strengthening Concrete*, Proceedings of the International Conference, Concrete 2000, Economic and Durable Construction Through Excellence, London, Vol. 1, pp. 239□253, 1993.

[20] Sharif, A., Al-Sulaimani, G. L., Basunbul, I. A., Baluch, M. H., and Ghaleb, B. N., *Strengthening of Initially Loaded Reinforced Concrete Beams Using FRP Plates*, ACI Structural Journal, Vol. 91, No. 2, pp. 160□168, 1994.

[21] Hutchinson, A. R. and Rahimi, H., *Behavior of Reinforced Concrete Beams with Externally Bonded Fibre Reinforced Plastics*, Proceedings of the 5th International Conference on Structural Faults and Repair, University of Edinburgh, Vol.3, pp. 221□228, 1993.

[22] DOT-Federal Highway Administration, *Fiber Reinforced Polymer Composites Application in USA*, Proceedings of the 1st Korea/U.S.A Road Workshop, Washington, D. C., 1997.

[23] American Concrete Institute (ACI), *Guide for the Design and Construction of Externally Bonded FRP Systems for Strengthening Concrete Structures (ACI 440.2R-02)*, Farmington Hills, Michigan, 2002.

[24] Fédération Internationale du Béton (fib), *Design and Use of Externally Bonded FRP Reinforcement for RC Structures*, FIB Bulletin 14, Lausanne, Switzerland, 2001.

[25] Teng, J. G., Smith, S. T., Yao, J., and Chen, J. F., *Intermediate Crack-Induced Debonding in RC Beams and Slabs*, Construction and Building Materials, Vol. 17, No. 6□7, pp. 447□462, 2003.

[26] Teng, J. G., Chen, J. F., Smith, S. T., and Lam, L., *FRP: Strengthened RC Structures*, John Wiley & Sons, Ltd, Chichester, UK, 2002.

[27] Chen, J. F., Yang, Z. J., and Holt, G. D., *FRP or Steel Plate-to-Concrete Bonded Joints: Effect of Tests Methods On Experimental Bond Strength*, Steel Composite Structure, Vol. 12, 231□244, 2001.

[28] Maeda, T., Asano, Y., Sato, Y., Ueda, T., and Kakuta, Y., *A Study on Bond Mechanism of Carbon Fiber Sheet*, Proceedings of the 3rd International Symposium on Non-metallic (FRP) Reinforcement for Concrete Structures (FRPRCS-3), Japan Concrete Institute, Sapporo, Vol. 1, pp. 279□286, 1997.

[29] Brosens, K. and Van Gemert, D., *Anchoring Stresses between Concrete and Carbon Fiber Reinforced Laminates*, Proceedings of the 3rd International Symposium on Non-metallic (FRP) Reinforcement for Concrete Structures, Japan Concrete Institute, Sapporo, Vol. 1, pp. 271□278, 1997.

[30] De Lorezis, L., Miller, B., and Nanni, A., *Bond of Fiber-Reinforced Polymer Laminates to Concrete*, ACI Material Journal, Vol. 98, No. 3, pp. 256□264, 2001.

[31] Nakaba, K., Kanakubo, T., Furuta, T., and Yoshizawa, H., *Bond Behavior between Fiber-Reinforced Polymer Laminates and Concrete*, ACI Structural Journal, Vol. 98, No. 3, pp. 359□367, 2001.

[32] Wu, Z., Yuan, H., Yoshizawa, H., and Kanakubo, T., *Experimental/analytical Study on Interfacial Fracture Energy and Fracture Propagation along FRP-Concrete Interface*, ACI International SP-201-8, Vol. 201, pp. 133□152, 2001.

[33] Dai, J. G. and Ueda, T., *Local Bond Stress Slip Relations for FRP Sheets-Concrete Interfaces*, Proceedings of the 6th International Symposium on FRP Reinforcement for Concrete Structures, World Scientific Publications, Singapore, pp. 143□152, 2003.

[34] Ueda, T., Dai, J. G., and Sato, Y., *A Nonlinear Bond Stress–Slip Relationship for FRP Sheet–Concrete Interface*, Proceedings of the International Symposium on Latest Achievement of Technology and Research on Retrofitting Concrete Structures, JCI, pp. 113□120, 2003.

[35] Pellegrino, C. and Modena, C., *Bond-slip Relationships between FRP Sheets and Concrete*, Proceedings of the 4th International Conference on FRP Composites in Civil Engineering (CICE2008), Zurich, Switzerland, 2008.

[36] Holzenkämpfer, P., *Ingenieurmodelle des Verbunds geklebter Bewehrung für Betonbauteile (PhD Dissertation)*, Technische Universität of Braunschweig, Braunschweig, 1994.

[37] Neubauer, U. and Rostásy, F. S., *Design Aspects of Concrete Structures Strengthened with Externally Bonded CFRP-Plates*, Proceedings of the 7th International Conference on Structural Faults and Repair, Vol. 2, pp. 109□118, 1997.

[38] Yuan, H., Wu, Z. S., and Yoshizawa, H., *Theoretical Solutions on Interfacial Stress Transfer of Externally Bonded Steel/Composite Laminates*, Journal of Structural Mechanics and Earthquake Engineering, JSCE, No. 675, pp. 27□39, 2001.

[39] Popovics, S., *A Numerical Approach to the Complete Stress-Strain Curve of Concrete*, Cement and Concrete Research, Vol. 3, No. 5, pp. 583□599, 1973.

[40] Kanakubo, T., Furuta, T., and Fukuyama, H., *Bond Strength between Fiber-Reinforced Polymer Laminates and Concrete*, Proceedings of the 6th International Symposium on Fibre-Reinforced Polymer (FRP) Reinforcement for Concrete Structures (FRPRCS-6), pp. 133□142, 2003.

[41] Guo, Z. G., Cao, S. Y., Sun, W. M., and Lin, Y., *Experimental Study on Bond Stress-Slip Behavior between FRP Sheets and Concrete*, Proceedings of the International Symposium on Bond Behavior of FRP in Structures (BBFS 2005), International Institute for FRP in Construction, Hong Kong, China, 2005.

[42] Pham, B. H. and Al-Mahaidi, R., *Modeling of CFRP-Concrete Shear-Lap Tests*, Construction and Building Materials, Vol. 21, No. 4, pp. 727□735, 2007.

[43] Ferracuti, B., Savoia, M., and Mazzotti, C., *Interface Law for FRP-Concrete Delamination*, Composite Structures, Vol. 80, No. 4, pp. 523□531, 2007.

[44] Mazzotti, C., Savoia, M., and Ferracuti, B., *An Experimental Study on Delamination of FRP Plates Bonded to Concrete*, Construction and Building Materials, Vol. 22, No. 7, 1409□1421, 2008.

[45] Chen, J. F. and Teng, J. G., *Anchorage Strength Models for FRP and Steel Plates Bonded to Concrete*, ASCE Journal of Structural Engineering, Vol. 127, No.7, pp. 784□791, 2001.

[46] Sato, Y., Asano, Y., and Ueda, T., *Fundamental Study on Bond Mechanism of Carbon Fiber Sheet*, Concrete Library International, JSCE, Vol. 37, pp. 97□115, 2001.

[47] Yoshizawa, H., Wu, Z., Yuan, H., and Knakubo, T., *Study on FRP-Concrete Interface Bond Performance*, Transactions of JSCE, Vol. 49, No. 662, pp. 105□119, 2000.

[48] Brosens, K. and Van Gemert, D., *Stress Analysis in the Anchorage Zones of Externally Bonded CFRP Laminates*, Proceedings of the International Conference on Infrastructure Regeneration and Rehabilitation – Improving the Quality of Life Through Better Construction, A Vision for the Next Millennium, Sheffield, pp. 931□940, 1999.

[49] Neubauer, U. and Rostásy, F. S., *Bond Failure of Concrete Fiber Reinforced Polymer Plates at Inclined Cracks—Experiments and Fracture Mechanics Model*, Proceedings of the 4th International Symposium, Non-Metallic (FRP) Reinforcement for Concrete Structures, Baltimore, USA, pp. 369□382, 1999.

[50] Lu, X. Z., Teng, J. G., Ye, L. P., and Jiang, J. J., *Bond−Slip Models for FRP Sheets/Plates Bonded to Concrete*, Engineering Structures, Vol. 27, No. 6, 920□937, 2005.

[51] Dai, J., Ueda, T., and Sato, Y., *Development of the Nonlinear Bond Stress-Slip Model of Fiber Reinforced Plastics Sheet-Concrete Interfaces with a Simple Method*, Journal of Composites for Construction, Vol. 9, No. 1, pp. 52□62, 2005.

[52] Brosens, K., *Anchorage of Externally Bonded Steel Plates and CFRP Laminates for the Strengthening of Concrete Elements (PhD. Dissertation)*, Department of Civil Engineering, Katholieke University Leuven, Leuven, 2001.

[53] Ulaga, T., Vogel, T., and Meier, U., *The Bilinear Stress-Slip Bond Model: Theoretical Background and Significance*, Proceedings of the 6th International Symposium on FRP Reinforcement for Concrete Structures (FRPRCS-6), Singapore, Vol. 2, pp. 153□162, 2003.

[54] Karbhari, V. M., Niu, H., and Sikorsky, C., *Review and Comparison of Fracture Mechanics-Based Bond Strength Models for FRP-Strengthened Structures*, Journal of Reinforced Plastics and Composites, Vol. 25, No. 17, pp. 1757□1794, 2006.

[55] Yang, Q. F., Lu, X. H., and Xiong, G. J., *Double Pull Specimen More Suitable for Measuring Bond-Slip Relationship of FRP-to-Concrete Interface*, Journal of Central South University Technology, Vol. 17, pp. 400□405, 2010.

[56] Comité Euro-International du Béton, *CEB-FIP Model Code (CEB-FIP MC90)*, Bulletin D'Information, No. 215, Lausanne, 1993.

[57] GB 50010, *Code for Design of Concrete Structures*, China Building Industry Press, Beijing, 2002 [in Chinese].

[58] Yao, J., Teng, J. G., and Chen, J. F., *Experimental Study on FRP-to-Concrete Bonded Joints*, Composites: Part B, Vol. 36, No. 2, pp. 99□113, 2005.

[59] American Concrete Institute (ACI), *Building Code Requirements for Structural Concrete (ACI 318-11) and Commentary (ACI 318R-11)*, Farmington Hills, ACI, 2011.

[60] Boresi, P. A. and Chong, P. K., *Elasticity in Engineering Mechanics Second Edition*, John Wiley & Sons, Inc., New York, 2011.

[61] Beer, F. P., Johnston, E. R., Jr., DeWolf, J., and Mazurek, D., *Mechanics of Materials Sixth Edition*, McGraw-Hill Companies, Inc., New York, 2011.

[62] Toutanji, H., Han, M., and Elhem, G., *Interfacial Bond Strength Characteristics of FRP and RC Substrate*, Journal of Composites for Construction, Vol. 16, No. 1, pp. 35□46, 2012.

[63] Yuan, H., Teng, J. G., Seracino, R., Wu, Z. S., and Yao, J., *Full-Range Behavior of FRP-to-Concrete Bonded Joints*, Engineering Structures, Vol. 26, No. 5, pp. 553□565, 2004.

[64] Kosmatka, S. H. and Panarese, W. C., *Design and Control of Concrete mixtures 13th Edition*, Portland Cement Association, Skokie, Illinois, 1988.

[65] ACI Committee 210, *Guide for Selecting Proportions for High-Strength Concrete with Portland Cement and Fly Ash (ACI 211. 4R-93)*, American Concrete Institute, Detroit, Michigan, 1993.

[66] Mehta, P. K. and Monteiro, P. J. M., *Concrete: Microstructure, Properties and Materials Third Edition*, McGraw-Hill Companies, Inc., New York, 2006.

[67] Kjellsen, K. O, Monsøyb, A., Isachsenb, K., and Detwilerc, R. J., *Preparation of Flat-Polished Specimens for SEM-Backscattered Electron Imaging and X-Ray Microanalysis—Importance of Epoxy Impregnation*, Cement and Concrete Research, Vol. 33, No. 4, pp. 611□616, 2003.

[68] Garbacz, A., Górka, M., and Courard, L., *Effect of Concrete Surface Treatment on Adhesion in Repair Systems*, Magazine of Concrete Research, Vol. 57, No. 1, pp. 49□60, 2005.

[69] Garbacza, A., Courardb, L., and Kostana, K., *Characterization of Concrete Surface Roughness and its Relation to Adhesion in Repair Systems*, Materials Characterization, Vol. 56, No. 4-5, pp. 281□289, 2006.

[70] Santosa, P. M. D., Júliob, E. N. B. S., and Silva, V. D., *Correlation between Concrete-to-Concrete Bond Strength and the Roughness of the Substrate Surface*, Construction and Building Materials Vol. 21, No. 8, pp. 1688□1695, 2007.

[71] Chajes, M. J., Finch, W. W., Jr., Januszka, T. F., and Thomson, T. A., Jr., *Bond and Force Transfer of Composite Material Plates Bonded to Concrete*, ACI Structural Journal, Vol. 93, No. 2, pp. 295□303, 1996.

[72] Täljsten, B., *Defining Anchor Lengths of Steel and CFRP Plates Bonded to Concrete*, International Journal of Adhesion and Adhesives, Vol. 17, No. 4, pp. 319□327, 1997.

[73] Ueda, T., Sato, Y., and Asano, Y., *Experimental Study on Bond Strength of Continuous Carbon Fiber Sheet*, Proceedings of the 4th International Symposium on Fiber Reinforced Polymer Reinforcement for Reinforced Concrete Structures SP-188, ACI, pp. 407□416, 1999.

[74] Zhao, H. D., Zhang, Y., and Zhao, M., *Research on the Bond Performance between CFRP Plate and Concrete*, Proceedings of the 1st Conference on FRP Concrete Structures of China, pp. 247□253, 2000.

[75] Adhikary, B. B. and Mutsuyoshi, H., *Study on the Bond between Concrete and Externally Bonded CFRP Sheet*, Proceedings of the 5th International Symposium on Fiber Reinforced Concrete Structures (FRPRCS-5), Cambridge, pp. 371□378, 2001.

[76] Xu, F., Chen, Y., and Guan, J., *Bond Strength between CFRP Sheets and Concrete*, Proceedings of the International Conference on FRP Composites in Civil Engineering, Hong Kong Institution of Engineers, Hong Kong Institution of Steel Construction, Hong Kong, pp. 357□364, 2001.

[77] Wu, Z., Yuan, H., Yoshizawa, H., and Kanakubo, T., *Experimental/Analytical Study on Interfacial Fracture Energy And Fracture Propagation along FRP-Concrete Interface*, ACI International Special Publication, Vol. 201, pp.133□152, 2001.

[78] Tan, Z., *Experimental Research for RC Beam Strengthened with GFRP (PhD Dissertation)*, Tsinghua University, Beijing, China, 2002.

[79] Ren, H. T., *Study on Basic Theories and Long Time Behavior of Concrete Structures Strengthened By Fiber Reinforced Polymers (PhD Dissertation)*, Dalian University of Technology, Liaoning, China, 2003.

[80] Sharma, S. K., Mohamed Ali, M. S., Goldar, D., and Sikdar, P. K., *Plate–Concrete Interfacial Bond Strength of FRP and Metallic Plated Concrete Specimens*, Composites: Part B, Vol. 37, No. 1, pp. 1□10, 2006.

[81] Toutanji, H., Saxena, P., Zhao, L., and Ooi, T., *Prediction of Interfacial Bond Failure of FRP−Concrete Surface*, Journal of Composites for Construction, Vol. 11, No. 4, pp. 427□436, 2007.